SAKARYA UNIVERSITY
INSTITUTE OF SCIENCE AND TECHNOLOGY

INVESTIGATION OF ELECTRO-MECHANICAL FACTORS EFFECTING MICRO-PUMP CHARACTERISTICS FOR BIOMEDICAL APPLICATIONS

Ph.D. THESIS

Hamid ASADI DERESHGI

Department	**:**	**MECHATRONICS ENGINEERING**
Field of Science	**:**	**MECHATRONICS ENGINEERING**
Supervisor	**:**	**Assist. Prof. Dr. Mustafa Zahid YILDIZ**

August 2019

SAKARYA UNIVERSITY
INSTITUTE OF SCIENCE AND TECHNOLOGY

INVESTIGATION OF ELECTRO-MECHANICAL FACTORS EFFECTING MICRO-PUMP CHARACTERISTICS FOR BIOMEDICAL APPLICATIONS

Ph.D. THESIS

Hamid ASADI DERESHGI

Department	:	**MECHATRONICS ENGINEERING**
Field of Science	:	**MECHATRONICS ENGINEERING**
Supervisor	:	**Assist. Prof. Dr. Mustafa Zahid YILDIZ**

This thesis has been accepted unanimously / with majority of votes by the examination committee on 06.08.2019.

Assist. Prof. Dr.
Mustafa Zahid YILDIZ
Head of Jury

Prof. Dr.
Durmuş KARAYEL
Jury Member

Prof. Dr.
Hakan Serhad SOYHAN
Jury Member

Prof. Dr.
İhsan PEHLİVAN
Jury Member

Assoc. Prof. Dr.
Cenk YAVUZ
Jury Member

DECLERATION

I declare that all the data in this thesis was obtained by myself in academic rules, all visual and written information and results were presented in accordance with academic and ethical rules, there is no distortion in the presented data, in case of utilizing other people's works they were refereed properly to scientific norms, the data presented in this thesis has not been used in any other thesis in this university or in any other university.

Hamid ASADI DERESHGI

06.08.2019

ACKNOWLEDGEMENTS

I would love to express my sincere gratitude, first and foremost, to my advisor Assist. Prof. Dr. Mustafa Zahid YILDIZ for encouraging me and for continuous support during my Ph.D. study and research. His guidance helped me during my research and writing of this thesis. I would like to thank to Prof. Dr. Durmus KARAYEL from Sakarya University of Applied Sciences and Prof. Dr. Hakan Serhad SOYHAN from Sakarya University for their helpful comments during my thesis progress.

I would like to express my thanks to Assoc. Prof. Dr. Nezaket PARLAK and Assoc. Prof. Dr. Mehmet Recep BOZKURT from Sakarya University for their help during the experiments. Part of the studies of this thesis was supported by Scientific Research Projects Unit of Sakarya University (Project Number: 2017-50-02-026) and Scientific Research Projects Unit of Sakarya University of Applied Sciences (Project Number: 2019-50-02-078).

TABLE OF CONTENTS

LIST OF SYMBOLS AND ABBREVIATIONS

D	: Diameter
E	: Young's modulus
f	: Darcy friction factor
g	: Acceleration of gravity
K	: Loss coefficient
L	: Length
M	: Bending moment
N	: Force
P	: Pressure
R	: Radius
s^E	: Elastic compliance constant
u	: Lateral displacement
v	: Fluid velocity
w	: Transverse displacement
z	: Height
Δh_{total}	: Total head loss
ε	: Strain
μ	: Poisson’s ratio
ρ	: Density
σ	: Stress
τ	: Shear stress
BDM	: Bi-diaphragm Micro-pump
CLPT	: Classical Laminated Plate Theory
MEMS	: Micro-Electro-Mechanical Systems
PZT	: Piezoelectric Zirconate Titanate
SDM	: Single Diaphragm Micro-pump

LIST OF FIGURES

LIST OF TABLES

SUMMARY

Keywords: Valveless Micro-pump, Bi-diaphragm, Piezoelectric Actuators, Fluid Flow Measurement, Displacement Measurement

In the past few decades, the advances in micro-electro-mechanical systems (MEMS) technologies have contributed to the rapid development of microfluidic devices in various functions. One of the important elements on MEMS is the micro-pump, which is capable of producing flow rates ranging in milliliter (ml) or microliter (μl) per minute. A commercial micro-pump should provide properties that justify the simple structure and miniaturization, high reliability, simple working principle, low cost and no need for complex controller. In this study, two novel piezoelectric actuated (lead zirconate titanate-PZT) valveless micro-pumps that can achieve high flow rates by pumping chambers and fixed reservoirs were designed and fabricated. Extensive experiments were conducted to investigate the effects of hydrodynamic and electromechanical on flow rates of the Single Diaphragm Micro-pump (SDM) and the Bi-diaphragm Micro-pump (BDM). BDM had two actuators facing to the same chamber at 180-degree phase shift. The primary features of the proposed designs were the high flow rates at low driving voltages and frequencies with the help of innovative design geometry. 3D-printing technique providing one-step fabrication for integrated micro-pumps with fixed reservoir was used. The micro-pump materials were biocompatible and can be used repeatedly to reduce costs. Mechanical parameters such as tensile test for silicon diaphragm, surface topography scanning by microscopy techniques and drop shape analysis for hydrophobic property were investigated to reveal surface wetting and flow stability. In addition, the effect of reservoir height was investigated and the calibration flow rates were measured during the inactive periods. The maximum diaphragm displacements were obtained at 45 V and 5 Hz. The maximum flow rate of SDM and BDM at 45 V and 20 Hz were 32.85 ml/min and 35.4 ml/min respectively. At all driving voltage and frequency levels, BDM had higher flow rates than of SDM.

BİYOMEDİKAL UYGULAMALARDA KULLANILAN MİKROPOMPALARIN KARAKTERİSTİĞİNİ ETKİLEYEN ELEKTRO-MEKANİK FAKTÖRLERİN İNCELENMESİ

ÖZET

Anahtar kelimeler: Valfsiz Mikropompa, Çift-diyafram, Piezoelektrik Aktüatörler, Akışkan Akışı Ölçümü, Deplasman Ölçümü

Geçtiğimiz birkaç on yılda, mikro-elektro-mekanik sistemler (MEMS) teknolojilerindeki gelişmeler, çeşitli fonksiyonlarda mikroakışkan cihazların hızlı gelişimine katkıda bulunmuştur. MEMS'teki önemli elemanlardan biri, dakikada mililitre (ml) veya mikrolitre (µl) arasında değişen debiler üretebilen mikropompadır. Ticari bir mikropompa, basit yapıyı ve minyatürleştirmeyi, yüksek güvenilirliği, basit çalışma prensibini, düşük maliyeti ve karmaşık denetleyiciye gerek duymayan gerekçeler sunmalıdır. Bu çalışmada, pompalama hazneleri ve sabit rezervuarlar ile yüksek debi elde edebilen iki yeni piezoelektrik aktüatörlü (kurşun zirkonat titanat-PZT) valfsiz mikropompa tasarlanmış ve imal edilmiştir. Tek Diyaframlı Mikropompa (TDM) ve Çift-Diyaframlı Mikropompa (ÇDM) akış hızları üzerindeki hidrodinamik ve elektromekaniksel etkileri araştırmak için kapsamlı deneyler yapılmıştır. ÇDM, 180 derecelik faz kaymasıyla aynı hazneye bakan iki aktüatöre sahiptir. Önerilen tasarımların temel özellikleri, yenilikçi tasarım geometrisi ile düşük giriş gerilimlerinde ve frekanslarda yüksek debilerdir. Sabit hazneli entegre mikropompalar için tek adımlı üretim sağlayan 3D baskı tekniği kullanılmıştır. Mikropompa malzemeleri biyolojik olarak uyumludur ve maliyetleri azaltmak için tekrar tekrar kullanılabilir. Silikon diyaframın çekme testi, mikroskopi teknikleri ile yüzey topografya taraması ve hidrofobik özellik için damla şekli analizi gibi mekanik parametreler yüzey ıslanma ve akış stabilitesini ortaya çıkarmak için incelenmiştir. Ek olarak, rezervuar yüksekliğinin etkisi araştırılmış ve giriş voltajının uygulanmadığı dönemlerde kalibrasyon debileri ölçülmüştür. Maksimum diyafram deplasmanı 45 V ve 5 Hz'de elde edilmiştir. TDM ve ÇDM'nin maksimum akış hızı, 45 V ve 20 Hz'de sırasıyla 32.85 ml/dak ve 35.4 ml/dak'dır. Tüm giriş voltaj ve frekans seviyelerinde, ÇDM, TDM'den daha yüksek debiye sahiptir.

CHAPTER 1. INTRODUCTION

This chapter of the thesis is prepared for better understanding and easier following of studies. The introduction of micro-pumps and explaining the reasons which specify the need for this fluid micro-instrument are the purpose of this chapter. Additionally, the components of the micro-pumps are fully explained in this chapter. Moreover, the advantages and disadvantages of the various components used to fabricate micro-pumps have been investigated according to the available information in the open literature. Finally, the reasons for choosing the type and material of the pieces used to fabricate presented micro-pumps are explained in this chapter.

1.1. Micro-pump

In the past few decades, the advances in micro-electro-mechanical system (MEMS) technologies have contributed to the rapid development of microfluidic devices in various functions [1, 2]. Some of the developed microfluidic devices are; micro-pump [3], micro-valve [4], micromixer [5], microchannel network [6], and a microfluidic flow sensor [7]. Micro-pumps are called heart of microfluidics [8]. Micro-pumps are able to carry fluids in small and accurate volumes [9]. Therefore, they have attracted the attention of industrial researchers and consumers [10]. Micro-pumps can be used to transfer small volumes of fluids in applications such as Microelectronics Cooling [11], Medical Systems [12], Chemical [13], Biological [14], and others [15, 16]. The first MEMS-based micro-pump was presented by Smits (1984) for insulin delivery systems to diabetic patients [17].

Working principles of the micro-pumps are quite different from the macro-pumps [18]. Additionally, micro-pumps can be classified from different typical specification.

Figure 1.1. indicate the broad classification of micro-pumps. In this study, the classification is based on the physical mechanism used in micro-pumps. Micro-pumps according to the physical mechanism are divided into two types, namely; mechanical and non-mechanical micro-pumps [19]. In the structure of mechanical micro-pump are moving mechanical parts, such as pumping diaphragms and check-valves. These mechanical parts are presented in Sections 1.2, 1.3 and 1.4 respectively. By contrast, in the structure of non-mechanical micro-pumps are not any mechanical parts to move the fluid. In these micro-pumps, the flow rate is obtained by hydrodynamic, electroosmosis or electrowetting effects [20].

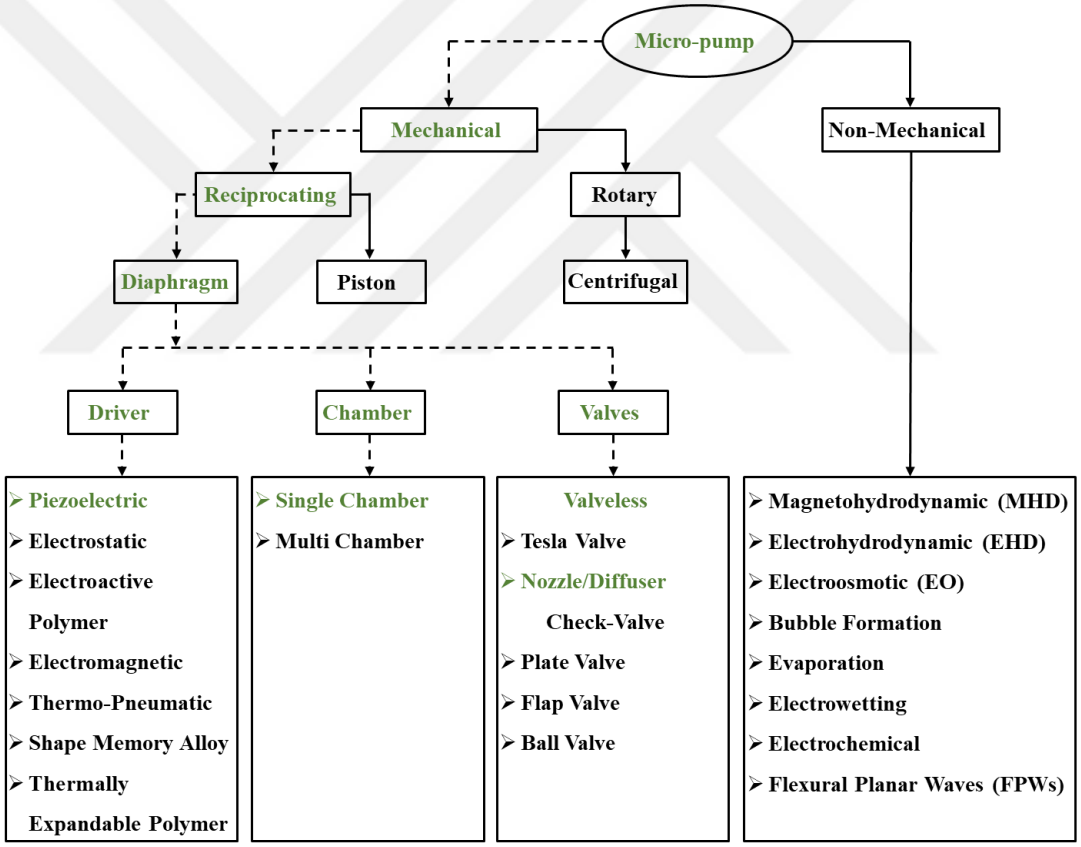

Figure 1.1. Classification of micro-pump

1.2. Actuators

Movement and mechanical control of a system is accomplished by actuators. A control signal and an energy source are required to activate the actuator. The control signal has relatively low energy and it may be in the form of electric voltage, pneumatic or hydraulic pressure or even human power. The energy source is usually electric, hydraulic fluid pressure, or pneumatic pressure. Additionally, in all micro-pumps an actuator is required to perform the pumping operation. In the literature, different actuators have been used to pump fluid by micro-pumps. In mechanical micro-pumps, fluid pumping is performed by physical actuators. The most common physical actuators include piezoelectric (PZT) [21], electrostatic [22], electromagnetic (EM) [23], electroactive polymer (EAP) [24], thermo-pneumatic [25], thermally expandable polymer [26], and shape memory alloy [27]. In non-mechanical micro-pumps, fluid pumping is performed by kinetic momentum. Non-mechanical micro-pumps convert non-mechanical energies to kinetic momentum. The most different types of driving mechanism include magnetohydrodynamic (MHD) [28], electrohydrodynamic (EHD) [29], electroosmotic (EO) [30], bubble formation [31], evaporation [32], electrowetting [33], electrochemical [34], and flexural planar waves (FPWs) [35].

1.2.1. Piezoelectric actuator

The ability of some materials and crystals which can convert mechanical energy into electrical energy and electrical energy into mechanical energy are called piezoelectric effect. Applying pressure causes electrical charge at the surface of the piezoelectric material. This phenomenon is called the direct piezoelectric effect. Moreover, applying electrical voltage causes piezoelectric deformation that is called reverse piezoelectric effect. The piezoelectric deflection rate depends on the amount of applied voltage and its direction. However, applying inverse pressure to piezoelectric material causes to reversed polarization of electrical charges. Additionally, the diversion of the applied electric field changes the direction of the piezoelectric material vibration. The deflection of piezoelectric materials is in micrometer or nanometer dimensions.

Piezoelectric actuators are some kind of microcontroller electromechanical systems. Most of the developed micro-pumps have used piezoelectric as an actuator. In terms of performance and size, piezoelectric pumps are reasonable [36]. Reverse piezoelectric effect causes suction and discharge in these micro-pumps. Applying an AC voltage causes the piezoelectric vibration in the horizontal direction. However, the piezoelectric actuator is tangentially glued onto the diaphragm (pumping membrane). Moreover, the side-edges of piezoelectric are clamped on the diaphragm. Accordingly, the piezoelectric horizontal deformation turns into a vertical vibration. The piezoelectric vertical vibration mode depends on the applied AC voltage behavior. The piezoelectric vertical vibration is transmitted exactly to the diaphragm because of being tangent. The vertical vibration of the diaphragm causes a periodic change in the volume of the chamber. Finally, periodic changes in the volume of the chamber produces oscillating flow rate in piezoelectric micro-pumps.

1.2.2. Electrostatic and electroactive polymer

Electrostatic forces are the dominant forces in interaction between particles in the intermediate-atomic dimension. Electrostatic phenomena are caused by forces that electrical charges apply on each other. Generally, there is a flexible diagram and a lower fixed substrate which are in parallel in the structure of electrostatic micro-pumps [37]. To vibrate the diaphragm in electrostatic micro-pumps, coulombic attraction should be provided between two oppositely-charged bodies [38]. Coulombic attraction causes the diaphragm vibration and alternating flow rate is produced in this type of micro-pumps.

Electroactive polymer (EAP) is a polymer component. Applying a voltage change the size and shape of this polymeric material. The most common application of this polymer is on actuators and sensors [39]. Recently, electroactive polymer materials are among the actuators used in the design of micro-pumps [40]. The Ionic Conductive Polymer Film (ICPF) or Ionic Polymer-Metal Composite (IPMC) are two common forms of this polymer actuator. This actuator has ability to achieve large deformations at low voltages [41].

1.2.3. Electromagnetic

Electromagnetic micro-pumps use electromagnetic mechanism to achieve flow rate. In this type of micro-pumps, two permanent magnets are placed on two opposite sides of the chamber. Additionally, the material of these micro-pumps' diaphragm should be selected from soft and elastic materials. Therefore, it can perform well due to electromagnetic field [42]. The diaphragm vibration of these micro-pumps is through the interaction between permanent magnets and a variable magnetic field achieved by a micro-coil [43]. Electromagnetic force can be attractive or repulsive. Therefore, by changing the current phase input, the diaphragm vibrates in the vertical direction. Eventually, the vibration of the diaphragm causes fluid flow generation.

1.2.4. Thermal actuations

Thermally actuated micro-pumps consist of thermo-pneumatic [44], shape memory alloy [45] and thermally expandable polymer [46]. Generally, thermo-pneumatic micro-pumps consist of a microheater, a diaphragm and a chamber. In these micro-pumps, the diaphragm is placed between the chamber and a microheater. Therefore, one side of diaphragm is in contact with the pump chamber and the other side of the diaphragm is face to face with microheater. The distance between the microheater and the diaphragm is gas or liquid mixture. The microheater heats the fluid that is between itself and the diaphragm. The heating of this fluid causes deformation of the diaphragm [47]. The diaphragm's deformation causes pressure changes in the pump chamber. Shape Memory Alloy (SMA) and bimetallic are thermal actuations. Both sensors have a shape memory effect and they are fabricated by special alloys. To vibrate these sensors high power (typically > 100 mW) is required. However, they can provide large force for the high-power consumption [48, 49]. Thermally expandable polymer is used as an actuator in diaphragm micro-pumps. In the structure of these actuators two materials with different thermal expansion coefficients are used and linked together. Due to temperature change, this sensor vibrates with high force but limited deflections [50, 51].

1.2.5. Magnetohydrodynamic (MHD)

Magnetohydrodynamics (MHD) is the science of studying the magnetic properties of electrically conductive fluid. MHD considers the interaction between ferromagnetic particles within the current and electromagnetic field. MHD is one of the most important methods of fluid pumping in non-mechanical micro-pumps. The pumping operation of MHD micro-pumps is carried out by Lorentz force. Lorentz force is obtained as a result of the interaction between the magnetic field and the electric field [52].

1.2.6. Electrohydrodynamic (EHD)

Electrohydrodynamic is the study of electrically charged fluid dynamics. Electro-hydrodynamic micro-pumps consist of one or more microchannels. The electrodes are placed along the microchannel. The fluid becomes charged by charging electrodes and creating an electric field. Eventually, the fluid moves due to the force applied by the electric field [53]. In EHD micro-pumps, a liquid with a low viscosity and high dielectric constant is required to achieve high flow velocity [54].

1.2.7. Electroosmotic (EO)

The external electric field causes fluid movement in electroosmotic micro-pumps. The electric field is applied through a channel with a charged wall [55]. In the channel design of the EO micro-pump, a silica or glass substrate with electrodes are used to generate an electric field through the channel [56]. In the literature, DC-operated fields or AC-operated fields are used for electroosmotic micro-pumps.

1.2.8. Bubble-type and evaporation-type micro-pumps

In bubble-type micro-pumps, bubbles arise due to the application of control voltage in micro-channels. Additionally, the application of the voltage causes periodic expansion and collapse of these bubbles, which causes the pumping operation in this type of

micro-pumps [57]. In evaporation-type micro-pumps, the xylem transport method is used for pumping operation. Xylem transport is a method in trees and vascular plants which is used to transfer water and minerals from the roots upwards. In these micro-pumps, Liquid evaporation is controlled by the membrane. Actually, the membrane directs the evaporation of the liquid to a gas space containing a sorption agent [58, 59].

1.2.9. Electrowetting (EW) and electrochemical micro-pumps

In electrowetting (EW) micro-pumps, the application of the voltage causes the wettability change of the surface which is usually hydrophobic. The voltage is applied to the dielectric layer in EW micro-pumps. Hence, the interfacial energy of the solid and liquid surfaces is reduced and it causes fluid transport under the effects of surface tension. This is because of the surface tension is an interfacial and dominant force [60].

In electrochemical micro-pumps, DC voltage is applied between two platinum electrodes in the salt water solution to obtain power. The applied DC voltage between electrodes trigger the produce of gas. Eventually, the generated electrochemical bubbles create a force for fluid movement [61].

1.2.10. Flexural planar waves (FPWs)

Flexural planar waves have been used in micro-pumps for fluid transport. In these micro-pumps, transducers are placed along the membrane. Transducers launch acoustic plate waves along the membrane and produce an acoustic field. Finally, the mechanism of acoustic stream causes fluid to be transported in this type of micro-pump [62].

1.3. Diaphragm

The diaphragm separates the fluid of micro-pump chamber from the actuator. Actually, the diaphragm is a flexible wall of the chamber and it is contacted with fluid inside the chamber. The side walls of the diaphragms are clamped to the housing of the micro-

pump. Hence, the diameter of the diaphragm is equal to the chamber's diameter. The actuator is located on the other side of the diaphragm. The actuator causes the diaphragm vibration in vertical direction. The vibration of the diaphragm causes the pressure difference in the chamber, and it causes fluid transport from reservoir to chamber and chamber to outlet.

In the fabricate of micro-pumps, one of the main parameters to be considered is the choice of diaphragm material. The diaphragm material must be selected relative to the application of the micro-pump. Moreover, in terms of cost and resistance against abrasion should be checked. Silicon [63-65], Beryllium bronze [66], Polyethylene Terephthalate (PET) [67, 68], SU8 [69], Brass [70], Parylene-C (PCPX)-Tetraethyl Orthosilicate (TEOS) [71], Nafion–Pt [72], Earthworm muscle [73], Polyimide [74], Elastomeric [75], Thermoplastic Polyurethane (TPU) [76], Polydimethylsiloxane (PDMS) [77, 78] and Soft Magnetorheological Elastomer (SMRE) [79] are diaphragm materials mainly used in the literature.

1.4. Micro-valves

Micro-pumps for net flow generation require some types of flow diodicity methods. Diaphragm displacement profiles are usually symmetrical which causes non-directional flow. Hence, the micro-valves are used for transforming the non-directional flow rate to directional one. Micro-valves are one of the important devices that most commonly used in microfluidic devices and mostly used in micro-pumps for the fluid transfer [80]. Generally, the micro-valves are classified as either check-valve [81] or valveless types [82].

The working principles of check-valves are similar to the diodes in the electrical circuit. There is only a small hydraulic resistance in the flow direction when the check-valve is placed forwardly. However, in the opposite direction it doesn't allow fluid to pass through. The check-valves use of plate [83], flap [84] and ball [85] to change the resistance. This mechanical diode has an important role in microfluidic transport systems. The check-valves transport the fluid in one direction. Check-valve type

micro-valves can avoid back flow but have a complicated structure [86]. However, there is a risk of valvular erosion and valve blockage by small particles or bubbles in liquids [87].

No-moving-parts (NMP) valves are especially qualified for fluid transfer in microfluidic systems. These valves have no mechanical moving parts to prevent back flow. These valves are used fluid properties for diodicity, instead of using mechanical moving parts. There are other advantages that justifies the use of these valves include simple structure and miniaturization, high reliability, simple working principle, low cost and no need for external control [88, 89]. In NMP micro-valves there are no moving mechanical piece. For this reason, the problems mentioned for check-valves do not exist in NMP micro-valves. Valveless type micro-valves cannot fully control the back flow and clogging, but their structure is simple comparing to check-valves [90]. Recently, different types of NMP valves have been presented. Stemme et al. (1993) proposed the first valveless micro-pump in 1993 [91]. A Tesla valve [92] and nozzle/diffuser elements [93] are NMP valves. The Tesla valve was invented in 1919 by Nikola Tesla [94]. In this type of valves, mechanical moving parts are not used to flow diodicity [95]. Tesla valve have a complicated structure, and this property causes different resistances to the fluid in the discharge and suction operation. The main property of Tesla valve diodicity arising from the angular differences of channels clash in two parts of the valve. The angular difference of channels collision causing more resistance of the back flow compared with the outlet flow [96]. Mohammadzadeh et al. (2014) investigated the effect of Tesla micro-valve and nozzle/diffuser element on micro-pump performance. The results show the superiority of Tesla valve in higher Reynolds number and its weakness in lower Reynolds number [97].

The working principle of both Tesla and nozzle/diffuser valves are dependent on fluid inertia and viscosity [98]. The flow diodicity in nozzle/diffuser elements is based on their structural difference. Diffuser is an enlarged channel in the flow direction. While, the nozzle has a decreasing cross section in the direction of flow [99]. Fluid velocity in nozzle is very high compared to the diffuser. Therefore, the output fluid has a higher-pressure drop-in nozzle than the diffuser. In other words, diffuser pressure drop is very

low compared to nozzle. Therefore, with constant pressure difference, the passing volumetric flow rate through the diffuser cross section is always greater than the nozzle cross section. In the designing of micro-pumps that use these elements as a micro-valve, the diffuser always selects the path of the reservoir to the chamber and the chamber path to the outlet. At the suction period, the fluid moves the diffuser path from the reservoir to the chamber, and at the discharge period, fluid again passes the diffuser path from the chamber to the outlet [100].

1.5. Chamber

In all micro-pumps, the fluids by activating the actuators and through the micro-valves are transmitted from the reservoir to the chamber. Finally, the fluid in the chamber is directed to the outlet channel. Accordingly, the dimensions and geometric shapes of the chamber affects the pressure characteristics, volume stroke and nozzle/diffuser loss coefficients.

Generally, micro-pumps' housing and chambers have been fabricated by common microfabrication technologies with polymethyl methacrylate (PMMA) [101], polydimethylsiloxane (PDMS) [102], pyrex glass [103] and silicon materials [104]. In open literature, most of the proposed micro-pumps have a chamber [105]. However, in order to increase the flow rate, some micro-pumps with two [106, 107] and three chambers [108, 109] are also presented in the papers. In Chapter 2, these designs have been investigated comprehensively.

1.6. Objectives

The purpose of this study was to design and fabricate two novels mechanical micro-pumps for biomedical applications. According to the literature survey, mechanical micro-pumps are more suitable for medical applications than non-mechanical micro-pumps. In non-mechanical micro-pumps, the fluid is affected by magnetic field, electric field, acoustic field or heat. The methods used to transfer fluid in non-mechanical micro-pumps may change the chemical properties of the drug.

In Section 2, the actuators which are presented in open literature for mechanical micro-pumps were investigated. Based on literature studies, piezoelectric can perform well compared to other mentioned actuators. As the piezoelectrics are quick to operate compared to other actuators. They produce a reasonably intermediate pressure against low energy consumption. Accordingly, the piezoelectric is a good actuator for micro-pumps designed for biomedical applications. Therefore, the piezoelectric actuator has been used in the presented designs.

In Section 4, the disadvantages and advantages of the various types of the micro-valves are investigated. Based on literature studies, nozzle/diffusor elements were used at the inlet and outlet of the fluid to the chamber. Moreover, the important parameters mentioned in the literature are considered to optimize the performance and compatibility of nozzle/diffusor elements with the proposed micro-pumps. These parameters are explained in Chapter 3. Additionally, biocompatibility is a very important key parameter that is necessarily considered for drug delivery micro-pumps. Silicon and PMMA are good biocompatible materials. Accordingly, the material of the diaphragms was silicon and the material of the housing and chamber was PMMA. It is worth noting, features of the provided micro-pumps components are examined in Chapter 3.

CHAPTER 2. PREVIOUS STUDIES

The purpose of this chapter is to obtain a more accurate insight and a clearer understanding relative to the research problem and the recognition of research gaps. Some of the studies available in the open literature that have novel innovations in the field of piezoelectric micro-pumps have been investigated in this chapter. Actually, some research gaps and unresolved issues are presented in this chapter. Finally, the novel piezoelectric micro-pump designs have been studied in this thesis and they are briefly described in this chapter. The methods and results of the previous studies were used in the design and fabrication of the proposed micro-pumps.

2.1. The Effects of Mechanical Factors on The Piezoelectric Micro-Pumps Performance

The first activities for the fabrication of micro-pumps started in the late 1980s [110-113]. Micro-pumps are an important part of MEMS which are used to pump up or control a very small volume of fluid. The transfer of medicine to the body with high perception and low cost has been one of the purposes of the micro-pump designers. Smits (1990) was the first piezoelectric micro-pump designer for drug delivery. The designated micro-pump was used is controlled insulin delivery systems for diabetic patients. This design reduced the need for continues needles injections in these patients [114]. In these applications, the transfer of large volumes of fluid to the body is not considered. Additionally, the pressure head is not the only indispensable indicator for pumping. Rather, high reliability, low energy consumption by the actuator, low fabrication cost and compatibility with biological conditions are also other basic parameters.

Generally, piezoelectric micro-pumps consist of a chamber, a diaphragm and two valves [115, 116]. In these micro-pumps piezoelectric clamp on the diaphragm and it vibrates the diaphragm. The movement of diaphragm put pressure on the fluid inside the chamber. The created alternating pressures cause the fluid suction from the reservoir to the chamber and the discharge of fluid from the chamber to the outside. In the following, some of the influential studies available in open literature has been briefly described.

Wang et al. (2006) investigated the effect of the membrane thickness and diameter, the piezoelectric thickness and diameter and the diameter of the chamber on the deflection by simulation. In this study, they proved that by increasing the thickness of the membrane the deflection decreases. On the other hand, they showed that thin membranes can have a lack of stiffness. The study demonstrated that the piezoelectric thickness must be higher than the thickness of the membrane. Additionally, the piezoelectric actuators have low mechanical strength. Therefore, the high increase of piezoelectric thickness reduces the deflection. The ratio of the membrane and piezoelectric dimensions should be considered according to the micro-pumps design. In this study, they proved that the diameter of the chamber was directly correlated with the deflection of the diaphragm. Increasing the diameter of the chamber caused an increase in the diaphragm deflection. The schematic of this micro-pump was shown in Figure 2.1.a [117].

Cui et al. (2007) presented a piezoelectric micro-pump for drug delivery applications. Two-dimensional structure schematic of this micro-pump was shown in Figure 2.1.b. In this study, the effect of mechanical factors of the diaphragm and piezoelectric actuator on diaphragm displacement, pump pressure and pump flow rate were investigated. The results showed that increasing the diaphragm thickness reduces displacement. Moreover, diaphragm displacement reduction reduces pump pressure and flow rate in the diaphragm micro-pump. Therefore, they proposed the thin diaphragm to increase the pump pressure [118].

Wang et al. (2014) presented a piezoelectric micro-pump with a folded vibrator for fuel delivery application. The proposed piezoelectric micro-pump was shown in Figure 2.1.c. The components of this micro-pump were a folded piezoelectric vibrator, a silicon diaphragm, a chamber, two PDMS check-valves, and two compressible spaces. The novelty of this work was to design and fabricate folded vibrators and compressible spaces near check-valves. The vibrator has three folded layers which a piezoelectric actuator was attached on each layer. The introduced novel vibrator increased diaphragm displacement. Additionally, the compressible spaces that were designed along with the check-valves could do shrink or expand. The liquid load was reduced because of the compressible spaces along the channels. Consequently, the flow rate was increased in the channels due to the reduced fluid loading. In this study, the maximum displacement was obtained 425 μm at 80 V_{P-P}, additionally, the maximum flow rate was 118 ml/min which obtained at 120 V_{P-P} and 361 Hz [119].

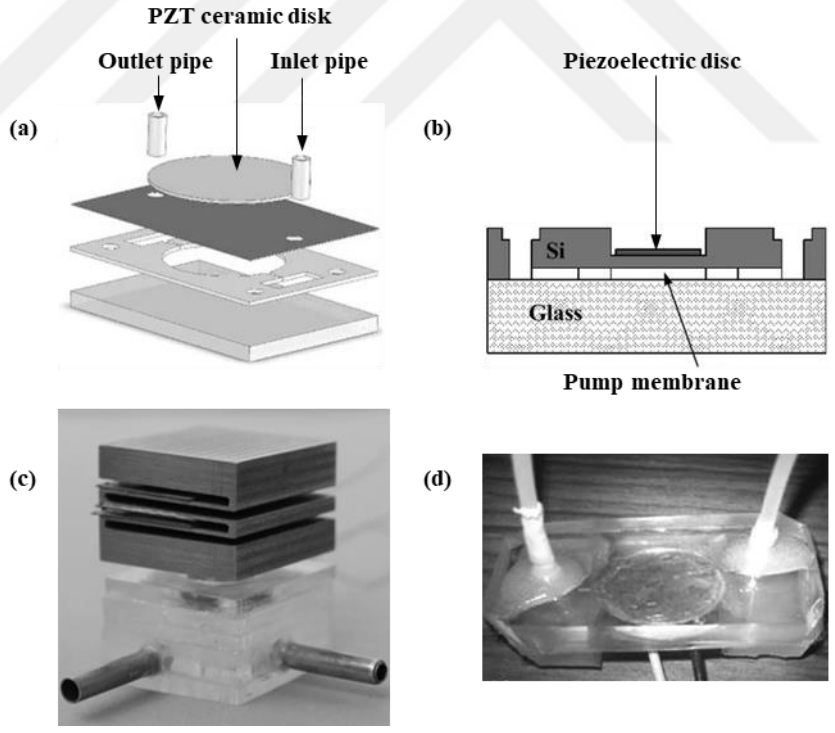

Figure 2.1. Investigation of mechanical factors affecting micro-pump performance by a) Wang et al. (2006) (Source: Reprinted from Ref. [117]), b) Cui et al. (2007) (Source: Reprinted from Ref. [118]), c) Wang et al. (2014) (Source: Reprinted from Ref. [119]), and d) Singh et al. (2015) (Source: Reprinted from Ref. [120])

Singh et al. (2015) investigated the effects of micro-pumps' components by simulation and experimental methods. The important factors affecting the flow rate including the nozzle/diffuser angle, the diameter and height of the chamber, the diameter and thickness of the diaphragm were investigated. The maximum flow rate of this micro-pump was 20 μL/min which was obtained at 30 V. The proposed piezoelectric micro-pump was shown in Figure 2.1.d [120].

2.2. The Effects of Electrical Factors on The Piezoelectric Micro-Pumps Performance

In piezoelectric micro-pumps, the diaphragm behavior depends on the voltage, frequency, phase, and wave shape of the AC voltage which apply to the piezoelectric actuator. In the open literature, the influence of electrical parameters has been investigated on the performance of the piezoelectric micro-pumps. In this section, some of the influential studies are briefly presented. For example; Fan et al. (2005), simulated a classic piezoelectric micro-pump and investigated the effect of the diaphragm vibrational frequency on the flow rate. The flow rate increased with the growth of the piezoelectric vibrational frequency and the maximum flow rate was obtained at the piezoelectric resonance frequency. It is worth noting that the frequency specifies the number of vibrations and the voltage determines the amplitude of the diaphragm deflection. Moreover, the peak deflection amplitude of the piezoelectric is at the resonance frequency. In this study, the highest flow rate was obtained at the resonance frequency. Additionally, they showed that if the application of the vibrational frequency is higher than the piezoelectric resonance frequency, causes a drop in the flow rate. Because the deflection amplitude decreases after the resonance frequency and causes a drop in the flow rate [121].

Wu et al. (2006) vibrated a check-valve type micro-pump’s diaphragm with a bimorph type piezoelectric actuator. This diaphragm’s actuator was fabricated from two piezoelectric actuators which were placed parallel to each other. The schematic of this micro-pump was shown in Figure 2.2.a. In this study, bimorph type piezoelectric actuator was used to increase diaphragm displacement force at low voltages. The

micro-pump performance was investigated by the vibration of the diaphragm in sine and square waves. Finally, they achieved a high flow rate with minimal energy consumption. The obtained maximum flow rate with the diaphragm vibration in the range of 20 Hz-70 Hz for a square and sinusoidal wave was 3 c.c./min and 2.3 c.c./min respectively [122].

Eladi et al. (2014) designed and fabricated a valveless micro-pump with PZT actuator. The schematic of the assembled micro-pump was shown in Figure 2.2.b. In their design, three distinct layers were used consisting of two layers of silicon and a layer of glass. These three layers were covered on top of each other and a composite structure was created. Water and methanol fluid were selected for pumping process. They investigated the effects of nozzle/diffuser, micro-pump chamber height, voltage, and frequency of the vibrating diaphragm elements of the net flow rate. For this micro-pump, the ideal voltage and frequency were achieved at 80 V and 250 Hz, respectively. In the ideal condition of pumping process, back pressure for water was zero and for methanol, 360 Pa [123].

Cazorla et al. (2016) investigated the effect of the diaphragm vibrational frequency on the flow rate. Additionally, the actuation voltage for piezoelectric at different frequencies was 24 V. In this study, the maximum deflection had been at the center of the diaphragm which was 5.6 μm. In this micro-pump, the flow rate was linearly increased to 0.8 Hz and it was sub-linearly from 0.8 Hz to 1 Hz. The maximum flow rate was obtained at 1 Hz which was 3.5 μl/min. The main advantage of this study was the ability of this micro-pump to operate at low voltages and low power consumption. Figure 2.2.c shows the proposed piezoelectric micro-pump and experimental set-up [124].

Revathi et al. (2018) proposed a composite-based piezoelectric micro-pump. The components of this micro-pump included an identical pair of nozzle/diffuser, a PDMS diaphragm, a chamber, and a piezoelectric actuator. The diaphragm and actuator diameters were exactly identical with the chamber diameter. The schematic of this micro-pump was shown in Figure 2.2.d.

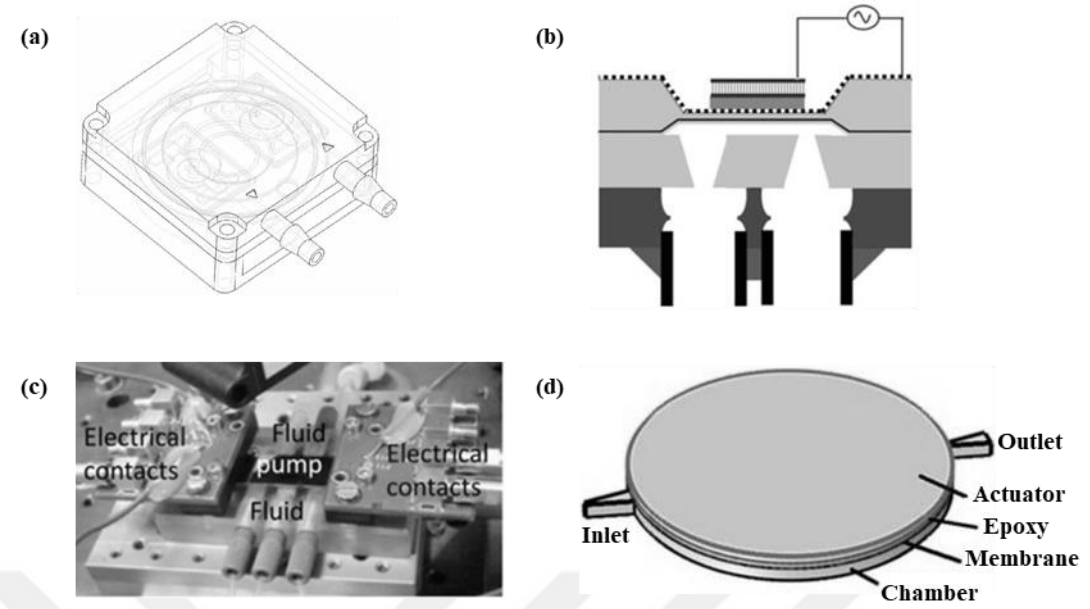

Figure 2.2. Investigation of electrical factors affecting micro-pump performance by a) Wu et al. (2006) (Source: Reprinted from Ref. [122]), b) Eladi et al. (2014) (Source: Reprinted from Ref. [123]), c) Cazorla et al. (2016) (Source: Reprinted from Ref. [124]), and d) Revathi et al. (2018) (Source: Reprinted from Ref. [125])

The purpose of this study was to obtain flow rates at low voltage and frequencies. Accordingly, the effect of voltage and frequency was investigated on flow rate. The flow rate was linearly increased in the range of 1 Hz-20 Hz, and the maximum flow rate was obtained at 20 Hz, that was 11.34 µl/min. In this micro-pump, the flow rate reduced at frequencies above 20 Hz. Piezoelectric actuator generated more force due to increased frequency. However, the pressure applied to the diaphragm has increased and it causes displacement to drop at higher frequencies than 20 Hz. Additionally, the flow rate of this micro-pump by increasing the voltage was increased linearly. Because, the amplitude of the diaphragm displacement was increased by increasing the voltage [125].

2.3. Mathematical Modeling of Multi-Layer Piezoelectric Actuator

The behavior of the piezoelectric actuators is affected by the actuator layers, fluid, and by their mechanical and electrical charge. According to the classical linear laminate plate theory (CLPT), the stress distribution along the plate thickness is assumed to be linear.

Using the CLPT hypothesis, Li et al. (2003) developed an analytical equation for the displacement of a circular piezoelectric actuator plate. They confirmed the displacement values they obtained by comparing them with the experimental results [126]. Mo et al. (2006) investigated the static displacement behavior of the unimorph circular diaphragm under electric charge analytically and experimentally. Other than electricity and fluid load, it is obvious that the applied mechanical load will also affect the behavior of the actuator [127].

Dong et al. (2007) took into account the electric field strength and the mechanical load effect for the analytical solution of the static displacement of a circular piezoelectric actuator. They stated that for maximum fluid transport, there should be an optimum thickness ratio between the PZT and metal layers [128].

Deshpande et al. (2007) developed an analytical model for the static displacement of a multi-layer and two-stage circular piezoelectric actuator subjected to constant fluid pressure and voltage load, using the classical laminate plate theorem (CLPT). They verified the analytical model outputs with finite element method and experimental study [129]. Wang et al. (2010) also developed the analytical static displacement model for the circular piezoelectric unimorph actuators, which were subjected to voltage load, using CLPT and verified by experimental studies. By the analytical model they established, they examined the changes in the structural parameters and material properties of the actuator [130].

Boundary conditions are also known to have a significant effect on the behavior of piezoelectric actuators [131]. Oniszczuk et al. (1998) analytically solved the transverse vibration problem of the elastic layer rectangular compound membrane system using the Bernoulli Fourier method [132]. Analytical modeling of the nonlinear dynamic behavior of valveless micro-pumps involving fluid interaction was described by Pan et al. (2001). They used the Galerkin and perturbation method for the analytical solution of the micro-pump under constant pressure [133]. Optimization of the electromechanical coupling coefficient of very thin piezoelectric devices was performed by Cho et al. (2005) [134]. Yu et al. (2005) investigated the dynamic

behavior of a prestressed diaphragm. They presented a mechanical diaphragm plate model subjected to a state of plane stress. They examined the membrane-like behavior of this diaphragm plate model and showed that the diaphragm exhibited different behavior, such as a plate or membrane, depending on the stress value [135].

For optimum fluid transfer of actuators, vibration frequency and modes should be determined. For this purpose, Olfatnia et al. (2010) investigated the vibrational modes and frequencies of circular piezoelectric micro diaphragms [136]. Vibration analysis of a circular micro-pump diaphragm were analyzed analytically and experimentally by Kaviani et al. (2014) [137], Esfahani et al. (2016 and 2018) [138, 139] and He et al. (2017) [140]. Hu et al. (2017) theoretically, numerically and experimentally studied the vibration parameters of circular type piezo-actuators with mass [141].

2.4. Peristaltic Piezoelectric Micro-pumps

In this type of design, more than one piezoelectric actuator is glued on a diaphragm, or several micro-pumps are connected in series. Additionally, AC voltages with different phases are applied to piezoelectric actuators. The piezoelectrics vibration with different phases causes pressure waves to the fluid inside the chamber. The pressure waves create a steady and propulsive movement in the fluid flow. In the literature, typically peristaltic piezoelectric micro-pumps are used to pump clean and sterile fluids. Therefore, the fluid movement is always prompter in these micro-pumps. As a result, the contamination can't be entered into the output channel direction. Accordingly, these types of micro-pumps are suitable for biomedical applications. There are many studies in literature, for example; Nguyen et al. (2008) fabricated a peristaltic micro-pump for biomedical applications. The proposed micro-pump was shown in Figure 2.3.a. In general, this micro-pump consisted of a chamber, two valves and three mini-LIPCA (lightweight piezo-composite actuators). It is worth noting that a LIPCA is a multi-layer composite actuator consisting of composite glass-epoxy layers, carbon-epoxy layers, and PZT ceramic wafer. In the presented study, three mini LIPCAs were attached on a diaphragm. Additionally, the same sinusoidal voltage and frequency were applied for each of the three LIPCAs. However, all three LIPCAs

vibrated with 120-degree phase shift to perform the peristaltic movement. Finally, the maximum obtained flow rate was 900 µl/min [142].

Jang et al. (2008) fabricated a three-chamber micro-pump connected by channels in series. The mechanical structure of the fabricated peristaltic piezoelectric micro-pump was shown in Figure 2.3.b. A silicon, Pyrex glass and piezoelectric actuator were the main components of this micro-pump. The chambers and channels were fabricated of silicon and the diaphragm was fabricated of Pyrex. A square piezoelectric actuator with a thickness of 191 µm was attached on each diaphragm. The same voltages and frequencies were applied to piezoelectric actuators. However, AC voltage with different phases was applied to piezoelectric to perform peristaltic motion. The maximum displacement and flow rate were obtained at 100 V_{P-P} and 100 Hz, which was 2.91 µm and 17.58 µl/min, respectively [143].

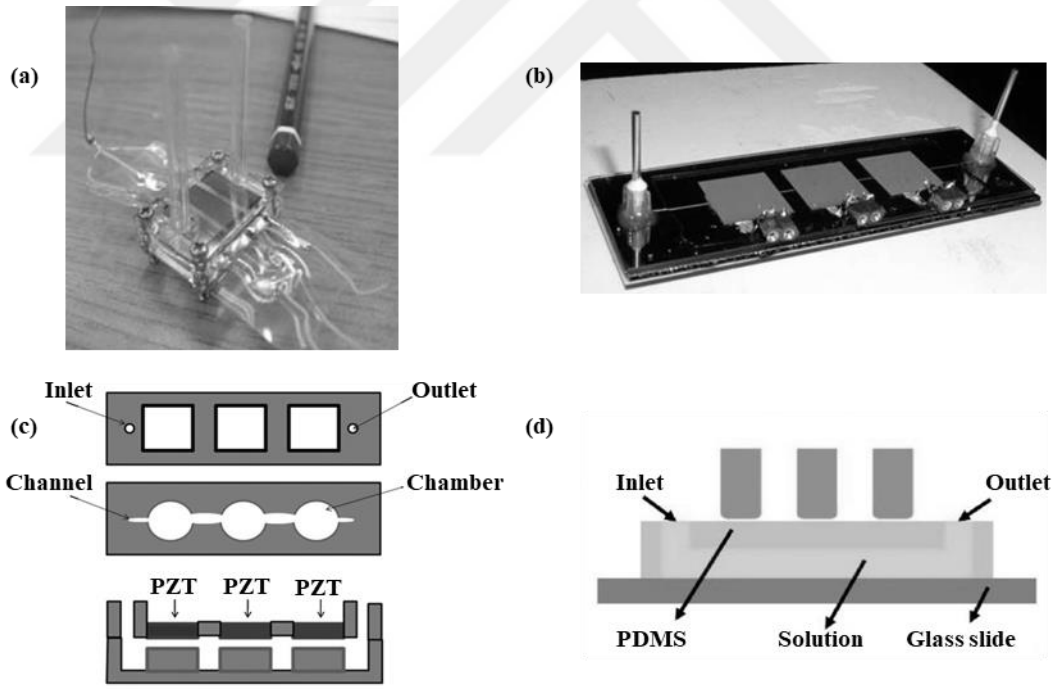

Figure 2.3. Structure of peristaltic piezoelectric micro-pump by a) Nguyen et al. (2008) (Source: Reprinted from Ref. [142]), b) Jang et al. (2008) (Source: Reprinted from Ref. [143]), c) Chao et al. (2011) (Source: Reprinted from Ref. [144]), and d) Ma et al. (2019) (Source: Reprinted from Ref. [145])

Chao et al. (2011) fabricated a micro-pump with three chambers connected in series and by channels. At the top of each chamber, a piezoelectric actuator was glued onto the diaphragm. The same voltage and frequency were applied to piezoelectric actuator. In order to perform a peristaltic motion, four-phase actuation sequence was selected which were in the form of 1 0 0–1 1 0–0 1 1–0 0 1. Here "1" showed the suction and "0" showed the discharge phenomena occurs. Figure 2.3.c shows the presented peristaltic micro-pump of Chao et al. (2011). In this study, they performed the charge recovery function using the driving circuit of the PZT actuator. The performance of this micro-pump at 80 V_{P-P} was increased by approximately 34% [144].

Ma et al. (2019) fabricated a peristaltic micro-pump which was integrated on a microfluidic chip. The schematic of this micro-pump was shown in Figure 2.3.d. The main components of this micro-pump were flexible microchannel, three piezoelectric actuator, PDMS diaphragm and micro pins. There were three micro pins on diaphragm each connected to a piezoelectric actuator. The piezoelectric actuator force transferred to the diaphragm by the pins. The pins vibrated the diaphragm of this micro-pump with T/6 phase shift. In this study, the two peristaltic micro-pumps outlet was connected to investigate the effect of voltage and frequency on the performance of the presented micro-pumps. One of the micro-pumps used blue dye water and another yellow dye water. For one of the micro-pumps blue dye water and for another yellow dye water were used. These dye waters passed a zigzag direction from the point where they were mixing together. They gained the effect of voltage and frequency on the performance of the micro-pump according to the water dye changes [145].

2.5. Piezoelectric Micro-pumps With Check-Valves

The check-valve, non-return valve or one-way valve is a kind of valve that allows the fluid to move in just one direction and completely prevents backflow. However, these valves have a complex structure and this issue was completely explained in Chapter 1. Easy fabricate is one of the important features in the micro-pump design. In this case, the miniaturization, care and maintenance of the micro-pump will be less problematic. The novel accomplished study on this project is based on valveless micro-pumps.

Therefore, in this study, these types of micro-pumps are more emphasized. However, there are many studies in the literature about piezoelectric micro-pumps with check-valves. In this section, important accomplished studies in this area are briefly reviewed.

Junwu et al. (2005) fabricated two piezoelectric cantilever-valve micro-pumps. The difference of these micro-pumps was in their cantilever-valves which were 2.5 mm and 3 mm respectively. The micro-pump with larger cantilever-valve had a higher flow rate. The schematic of the cantilever valve was shown in Figure 2.4.a [146].

Ma et al. (2008) fabricated a one-sided actuating piezoelectric micro-pump for a closed water-cooling system. The chamber of this micro-pump constructed of an aluminum by CNC machine. In this study, check-valve which was in the form of a cantilever beam were used in the pump chamber. The material of the check-valve and diaphragm in this micro-pump was PDMS. The working principle of the investigated valve was shown in Figure 2.4.b. The maximum flow rate for this micro-pump was 72 ml/min when ±50 V (AC) and 100 Hz applied to the piezoelectric actuator [147].

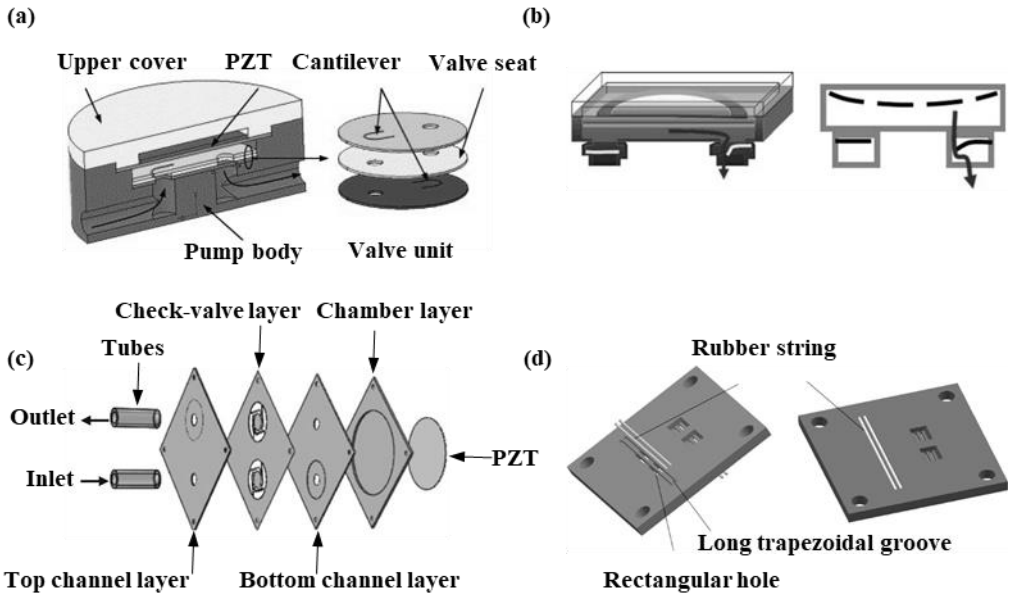

Figure 2.4. Mechanical structure of check-valve recommended by a) Junwu et al. (2005) (Source: Reprinted from Ref. [146]), b) Ma et al. (2008) (Source: Reprinted from Ref. [147]), c) Cheng et al. (2013) (Source: Reprinted from Ref. [148]), and d) Ren et al (2016) (Source: Reprinted from Ref. [149])

Cheng et al. (2013), used the check-valve in the proposed micro-pump for backflow management. An exploded view of this piezoelectric micro-pump was shown in Figure 2.4.c. The connected check-valves to the chamber were bridge-type. The working principle of these valves depended on the vibrational position of the diaphragm and performed the operation of opening and closing channels accordingly. Therefore, in the supply mode, the output channel closed and the input channel opened. In contrast, in the pump mode, the output channel was opened and the input channel was closed. The maximum flow rate of this micro-pump was obtained 1.82 ml/min at 120 V_{P-P} and 160 Hz [148].

Ren et al (2016), proposed the use of the string type check-valve for the inlet and outlet of the fluid into the chamber. The structure of the string type check-valve was shown in Figure 2.4.d. The components of this check-valve were a valve seat and flexible rubber strings. There were rectangular holes on the valve seat. These rectangular holes completely covered by rubber strings when the diaphragm did not vibrate and the pressure of the chamber was zero. The pressure changes inside the chamber caused the opening and closing of the rubber strings. In the supply mode, the rubber strings of the inlet channel were opening. In pump mode, the rubber strings of output channel were opening. In this micro-pump, the water was chosen for pumping operation. The maximum obtained flow rate was 67.1 ml/min, when the sinusoidal voltage of 170 V_{P-P} and 1 kHz were applied to the piezoelectric actuator [149].

2.6. Piezoelectric Micro-pumps With No-Moving-Part Valves

The structure of micro-valves has an important role in the micro-pump performance. Therefore, the discussed parameters in Chapter 1 including the diodicity capability and easy fabrication and another parameter should be considered in the selection of the valves. In Chapter 1, the mechanism of no-moving-parts valves was explained. Here, the application of nozzle/diffuser elements in piezoelectric micro-pumps and the innovations that were used in their structure are explained briefly.

The first idea of using no-moving-part valves was presented by Goran Stemme and Eric Stemme in 1993 [91]. They fabricated a piezoelectric micro-pump and they used nozzle/diffuser elements for flow diodicity. They obtained useful experimental data from this micro-pump. Other researchers have used these data in later works and studies. Experimental data showed that the flow rate diagram varies linearly with the pressure head for the micro-pump. The valveless micro-pumps investigated by many researchers. One of the most important studies was Forster et al. (1995) works. For the first time, they studied the viscosity loss and the dynamic drop-in nozzle/diffuser elements and Tesla valves [150].

Forster et al. (2002) proposed a Tesser valve with parametric design. The Tesser valve was performed from the combination of Tesla valve geometry and nozzle/diffuser elements. Thus, the Tesser valve was more complex than the nozzle/diffuser elements and Tesla valves and had many independent geometric parameters. The two-dimensional schematic of the Tesser valve was shown in Figure 2.5.a. In this study, the Tesser valve performance was compared with the nozzle/diffuser elements and a Tesla valve. The simulation results showed that the performance of nozzle/diffuser elements and tesla valve were better than Tesser valve. Additionally, the simulation results determined that nozzle/diffuser elements in the low Reynolds number ($Re < 100$) and tesla valves in the high Reynolds number ($Re > 100$) had better performance [151].

Cui et al. (2008) proposed a valveless piezoelectric micro-pump and its performance was investigated by Finite Element Method (FEM). The two-dimensional schematic of the nozzle/diffuser element was shown in Figure 2.5.b. Their simulation results showed that at fixed frequencies, increasing the voltage increased the pump flow rate and the pressure. Additionally, increasing the length of the nozzle/diffuser element increased the flow rate and reducing the diffuser angle increased the net flow rate of the micro-pump. The outlined highlights of this micro-pump included high reliability, low sensitivity to drug particles, and good biocompatibility [152].

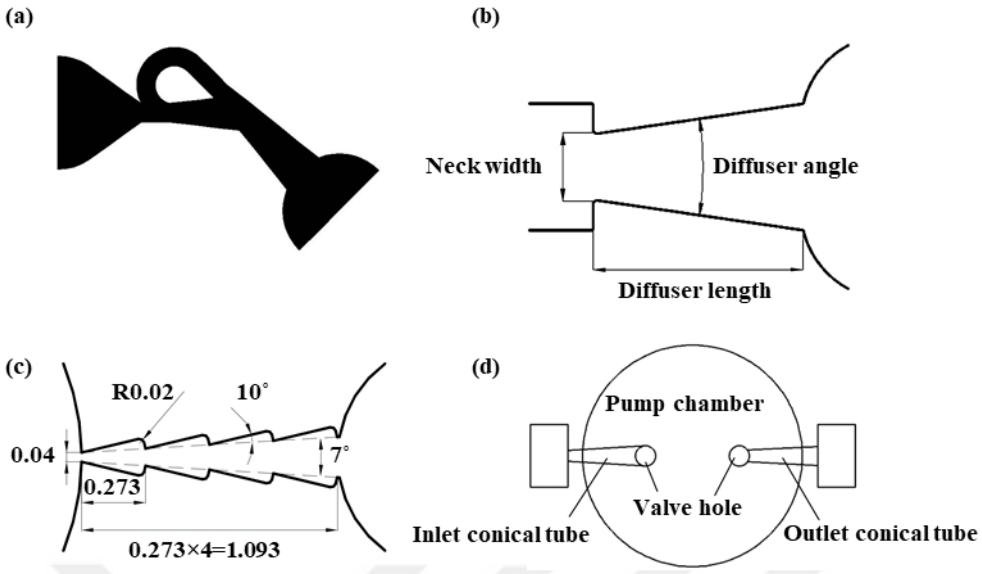

Figure 2.5. Mechanical structure of no-moving-part valve recommended by a) Forster et al. (2002) (Source: Reprinted from Ref. [151]), b) Cui et al. (2008) (Source: Reprinted from Ref. [152]), c) Guan et al. (2009) (Source: Reprinted from Ref. [153]), and d) Ji et al. (2019) (Source: Reprinted from Ref. [154])

Guan et al. (2009) fabricated silicon-based saw-tooth microchannels using Deep Reactive Ion Etching (DRIE) techniques. In this study, the performance of saw-tooth microchannel was compared with the performance of nozzle/diffuser elements at different voltages, frequencies, and driving signals. The maximum flow rate of the micro-pump with saw-tooth microchannel was 1.85 times higher than the micro-pump with the traditional nozzle/diffuser elements. The saw-tooth microchannel was shown in Figure 2.5.c [153].

Ji et al. (2019) simulated three piezoelectric micro-pumps in COMSOL Multiphysics and they fabricated the proposed micro-pumps. In this micro-pump, the piezoelectric actuator was clamped on the upper chamber wall and the nozzle/diffuser elements were connected to the lower wall of the chamber. The schematic of nozzle/diffuser elements and valve holes were shown in Figure 2.5.d. Two holes with a diameter of 3 mm performed in the lower wall for attaching nozzle/diffuser elements to the chamber. In this study, the effect of space of valve hole investigated on the performance of piezoelectric micro-pump. The performance of micro-pump was investigated in three different spaces of the holes and these spaces were 15 mm, 3 mm, and 25 mm. The maximum flow rate was obtained for the micro-pump with 3 mm hole space that it was

8.43 ml/min. The flow rate of this micro-pump toward the micro-pumps that the hole spaces were 15 mm and 25 mm was 13.6% and 47.1% higher respectively. It should be noted that the obtained results from the performance of this micro-pumps were almost identical in the simulation and numerical analysis method [154].

2.7. Multi-Chamber Piezoelectric Micro-pumps

Recently, the study of multi-chamber piezoelectric micro-pumps have received special attention. Due to the alternating flow rate, the application of single-chamber micro-pumps is limited. In the literature, the performance of multi-chamber and single chamber micro-pumps were compared. According to the studies, multi-chamber micro-pumps had good stability and high flow rate compared to single-chamber micro-pumps. There are many studies in the literature, for example; Lintel et al. (1988) proposed a two-chamber piezoelectric micro-pump. They fabricated this micro-pump based on micromachining of silicon technology. They also used passive silicon check-valves for diodicity of flow rate [155]. Cao et al. (2001) simulated a three-chamber piezoelectric micro-pump. The chambers were connected in series by channels. Figure 2.6.a shows the schematic of the proposed micro-pump. The inlet micro-valve of this micro-pump was attached to the left-handed chamber and the outlet micro-valve was attached to the right-handed chamber. Each chamber had a separate diaphragm and piezoelectric actuator. In this micro-pump, they were able to improve the flow rate by creating peristaltic motion [156].

Kan et al. (2008) fabricated a multi-chamber micro-pump to achieve a high flow rate at low voltage (see Figure 2.6.b). The housing of proposed micro-pumps fabricated from PMMA and the diameter of the chambers were 10 mm and their height was 0.2 mm. They used cantilever valves for fluid inlet and outlet in this micro-pump and the size of these valves was 4 mm × 1.35 mm. In this study, firstly, the effect of the number of chambers on the net flow rate was investigated. Secondly, the effect of frequency was studied on the net flow rate. Finally, the maximum flow rate was obtained 7.6 ml/min when the four piezoelectric micro-pumps were connected in series and 40 V and 300 Hz were applied to piezoelectric actuators [157].

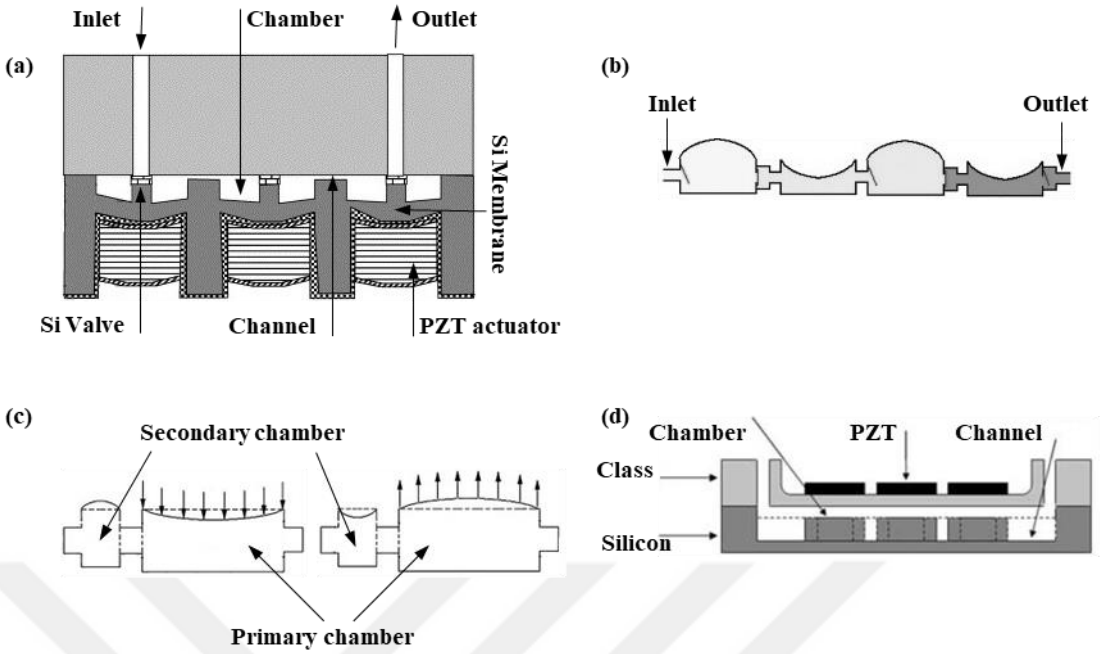

Figure 2.6. Design of the proposed multi-chamber piezoelectric micro-pump by a) Cao et al. (2001) (Source: Reprinted from Ref. [156]), b) Kan et al. (2008) (Source: Reprinted from Ref. [157]), c) Ma et al. (2011) (Source: Reprinted from Ref. [158]), and d) Jang et al. (2011) (Source: Reprinted from Ref. [159])

Ma et al. (2011) fabricated a one-sided actuating piezoelectric valveless micro-pump with a secondary chamber. In this paper, they proposed a two-chamber micro-pump that the secondary chamber located between the primary chamber and the output channel (see Figure 2.6.c). The upper part of two chambers was sealed by PDMS and a rectangular piezoelectric plate was glued on the diaphragm of the primary chamber. However, the diaphragm of the secondary chamber vibrated consonant with primary chamber diaphragm. Consequently, the maximum net flow rate was obtained 1.183 ml/s at 150 Hz. The net flow rate of this micro-pump due to the addition of a second chamber was increased to 0.989 ml/s [158]. Jang et al. (2011) proposed a three-chamber micro-pump that the diameter of all three chambers was 12 mm (see Figure 2.6.d). Glass was used as a diaphragm in this micro-pump. Additionally, square piezoelectric actuators with dimensions of 12 mm × 12 mm attached on the diaphragms. The sequences of 3-4 and 6 phase actuation was applied to perform peristaltic motion. The best performance of this micro-pump was in 6 phase sequence. The maximum net flow rate was obtained 36.8 µl/min at 100 V_{P-P} and 700 Hz [159].

2.8. Scope of The Thesis

Literature survey shows that there are many studies about the piezoelectric actuated diaphragm micro-pumps. For example, Zhang et al. (2013a) fabricated a single piezoelectric diaphragm micro-pump and used check-valves in the inlet and outlet of the chamber. In the presented study, the effects of voltages and frequencies that cause flow rate changes on the micro-pump were investigated. Therefore, the piezoelectric actuator was divided into two parts as driving unit and sensing unit. However, they did not report that use any isolating diaphragm between the piezoelectric actuator and water. The maximum flow rate was 45.98 ml/min which obtained at 150 V_{P-P} and 30 Hz, additionally, the sensing voltage achieves a maximum value of 3.02 V_{P-P} [160]. In addition, Zhang et al. (2013b) presented a prototype micro-pump with double piezoelectric diaphragm which serial connected. The size of the prototype micro-pump was 65 mm × 40 mm × 12 mm. They showed that the advantages of double actuator micro-pumps and maximum flow rate in prototype micro-pump was 45.98 ml/min which obtained at 200 V and 15 Hz [161]. For fuel delivery applications, Wang et al. (2014) fabricated a check-valve micro-pump was composed of three parts, namely, piezoelectric actuator, chamber and valves. The novelty of this work consists of compressible spaces made of PMMA plate that was mounted at the bottom of the micro-pump. As a result, the compressible spaces caused to increase flow rate. The maximum flow rate of 105 ml/min were obtained when the piezoelectric actuator was driven with 400 V_{P-P} and 490 Hz [162]. Ma et al. (2015a) reported a piezoelectric-based micro-pump for biomedical applications. They designed the chamber in the form of rib structures to direct the flow. Consequently, the maximum flow rate was reported as 196 ml/min at 70 V and 25 Hz [163]. Ma et al. (2015b) designed low flow piezoelectric micro-pump with check-valves. The chamber was fabricated from the PMMA and the diameter was 10 mm. The important highlight of this study was the new diaphragm model that fabricated a cylindrical protrusion had clamped to the center of the micro-pump's PDMS diaphragm. Additionally, the effects of chamber depth and diaphragm thickness on flow rate were investigated. As a result, the maximum obtained flow rate was 6.21 ml/min [164]. Pan et al. (2015) studied on the same micro-pump done by Wang et al. (2014). However, in this study a square wave

voltage and sinusoidal wave voltage were used to drive the piezoelectric actuator. Consequently, the performance of this micro-pump at the square wave voltage was much better than the sinusoidal wave voltage. Thus, the maximum flow rate was 163.7 ml/min when the piezoelectric actuator was driven with a square-wave voltage of 400 V_{P-P} and 445.5 Hz [165]. In another study of Ma et al. (2016) designed the valveless piezoelectric micro-pump for biomedical applications. The only difference was that the vibrator of the micro-pump was a piezoelectric bimorph actuator connecting with Polyethylene Terephthalate (PET) diaphragm. The maximum flow rate was 9.1 ml/min [166]. The paper of Okura et al. (2017) reported a microfluidic droplet creation device consisting of a PDMS microfluidic chip in the field of drug delivery. The maximum flow rate of this micro-pump was reported as 10 ml/min at 250 V_{P-P} and 60 Hz [167]. Eventually, Ye et al. (2018) fabricated a new micro-pump design by adding a thin steel blocking edge which was pressed perpendicularly to the center of the check-valve film. They reported that the flow rate increased by 40% - 300% and the maximum flow rate was obtained 187.2 ml/min [168].

Many studies have been carried out on micro-pumps. However, none of them contain detailed information about design parameters, mechanical and electrical effects on flow rates. In addition, new designs have been proposed by different researchers, but there are no studies supporting each other. In this study, two novel PZT based micro-pumps have been fabricated which can be used in a wide range of areas such as mechanical, energy and biomedical applications. The novelty of this study was that the BDM (Bi-diaphragm Micro-pump) and SDM (Single Diaphragm Micro-pump) had a fixed reservoir near the chamber to achieve portable and controllable features. Another geometric novelty was that the BDM consisted of a chamber sandwiched between two diaphragms actuated by two piezoelectric actuators at the same time to achieve high flow rate. According to literature survey, there is no similar micro-pump geometry in the presented studies. In order to compare the performance of the BDM, we fabricated the SDM with same geometric parameters and material. All the structure elements of the micro-pumps were selected as biocompatible. Therefore, the silicon was chosen as a diaphragm in these micro-pumps, and the PMMA was used to fabricate the chamber, nozzle/diffuser elements and reservoir. Profilometer, Scanning Electron Microscopy

and Field Emission Microscopy were used for surface roughness characteristics of the fabricated micro-pumps. Drop shape analysis was used to test hydrophobic or hydrophilic behavior of the PMMA material. At last, a tensile test was applied for elastic behavior of the silicon diaphragm. Consequently, experimental flow rates were measured and it was shown that BDM had higher flow rates at all frequency and voltage levels.

CHAPTER 3. MATERIALS AND METHODS

This chapter is the beating heart of the presented study. Because the stages of designing and fabricating processes of the novel micro-pumps are investigated in this chapter. Additionally, the different computational methods used in the study of the proposed micro-pumps are presented in this chapter. This chapter is organized as follows. The working principle of the novel piezoelectric micro-pumps is explained in Section 1. Additionally, the specifications of the material used in different parts of the micro-pumps are explained by reasons. The theoretical analysis of diaphragm is described in Section 2. The micro-pump calibration and flow test are explained in Section 3. Additionally, the theoretical analysis of microfluidic is described in Section 3.

3.1. Micro-pump Design and Working Principle

In this study, two novel piezoelectric actuated (lead zirconate titanate-PZT) valveless micro-pumps that can achieve high flow rates by pumping chambers and fixed reservoirs were designed and fabricated. The structure of piezoelectric micro-pumps was shown in Figure 3.1. These micro-pumps consist of fluid reservoir, chamber, nozzle/diffuser elements, silicon diaphragm and piezoelectric actuator. We fabricated the chamber, nozzle/diffuser and fluid reservoir in the clean room by using the Objet260 Connex3 Printer. The material of these elements was PMMA. Additionally, in this study, piezoelectric coated brass disks were used, which can be available commercially. Moreover, silicon diaphragm was the separator layer of piezoelectric actuator with water. To study the characteristics of the silicon diaphragm “Tensile Test” was performed. In addition, the silicon diaphragm properties can be summarized as; Young's modulus (162 GPa), Poisson's ratio (0.22) and density (2329 kg/m^3) respectively. The optimum nozzle diffuser divergence angle was reported 10-degrees [120]. Therefore, in this study the nozzle/diffuser divergence angle was chosen 10-

degrees. Inlet and outlet diameters of nozzle/diffuser elements were designed to be 0.2 mm and 2 mm, respectively. The height of the reservoir and radius were 20 mm and 25 mm, respectively. The geometric parameters of the micro-pumps' components were given in the Table 3.1.

As shown in Figure 3.1., the geometric and physical parameters of the two micro-pumps were exactly equal. The only difference between these two micro-pumps was in the number of diaphragms and the piezoelectric. Thus, that in the Single Diaphragm Micro-pump (SDM), in the upper part of the chamber, there was a silicon diaphragm and a piezoelectric actuator. While in the Bi-diaphragm Micro-pump (BDM), two silicon diaphragm and two piezoelectric actuators were used. In other words, our proposed configuration (BDM) consists of a chamber sandwiched between two diaphragms. Essentially, the novelty of this work was that the BDM had two vibrational diaphragms that were placed in parallel. Figure 3.2. shows the prototype micro-pumps fabricated by PMMA material.

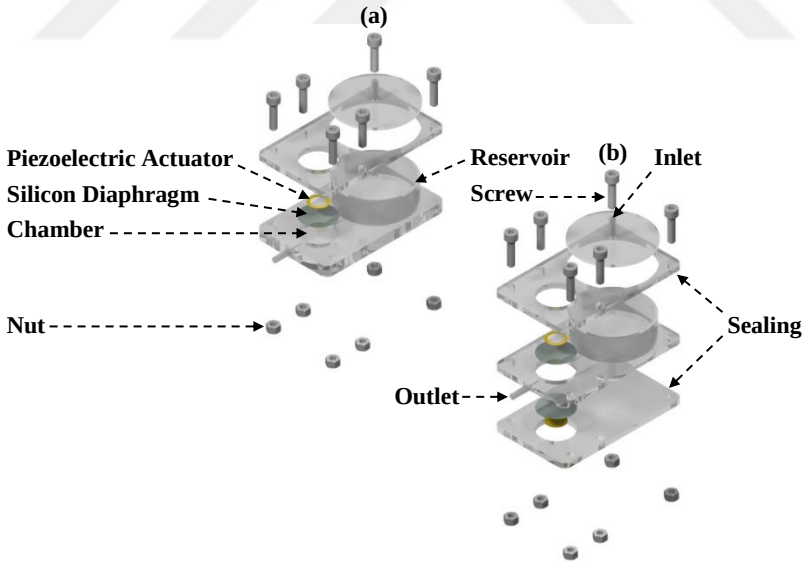

Figure 3.1. Exploded view of the micro-pumps, (a) SDM, (b) BDM

Table 3.1. The geometrical characteristics of micro-pumps components

Micro-pump component	Specifications (mm)
Chamber diameter (d_{Ch})	25
Chamber height (h_{Ch})	4
Nozzle diameter (d_N)	0.2
Diffuser diameter (d_D)	2
Silicon diaphragm diameter (d_S)	25
Silicon diaphragm thickness (t_S)	0.1
Piezoelectric actuator diameter (d_P)	14
Piezoelectric actuator thickness (t_P)	0.2
Reservoir height (h_R)	20
Reservoir diameter (d_R)	50

Figure 3.3. indicates the working principle of the proposed micro-pumps. The working principle and displacement measurement of the represented micro-pumps in this study were similar to the studies by [169, 170]. Applying alternative voltage causes piezoelectric deformation that is called reverse piezoelectric effect. The piezoelectric displacement rate depends on the amount of applied voltage and its direction. The mesh convergence method was used by COMSOL Multiphysics 4.3 to obtain required displacement amplitude of the diaphragm where the values were saturated. The working principle of piezoelectric actuators include two stages, namely, the discharge and the suction. By applying the sinusoidal voltage, the diaphragm vibrates. In the positive half-cycle of the sinusoidal voltage, the diaphragm bends upwards, and in this situation, the liquid suction was carried out from the reservoir to the chamber. In the negative half-cycle of the sinusoidal voltage, the diaphragm bends downward and the discharge of fluid from the chamber takes place. In this study, the same voltage and frequencies were applied to piezoelectric of both micro-pumps. However, the sinusoidal voltage was applied with 180-degrees phase shift to BDM's piezoelectric actuators. The phase shift increased the suction and discharge force of the BDM compared to the SDM. In other words, increasing discharge and suction force resulted in an increase in net flow rate. The net flow rate results were given in Chapter 4.

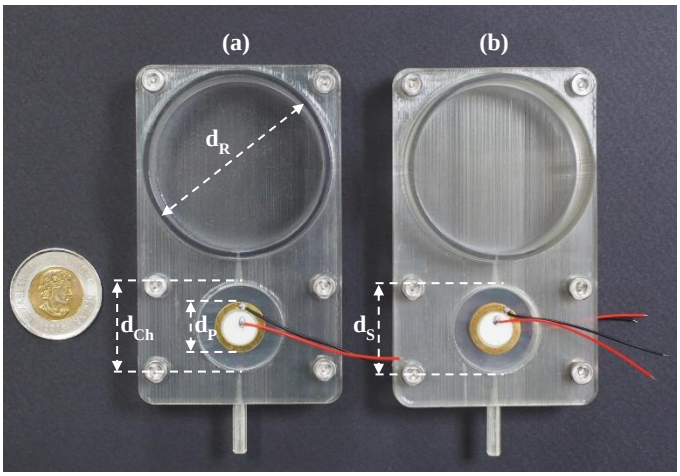

Figure 3.2. Fabricated micro-pumps, (a) SDM, (b) BDM

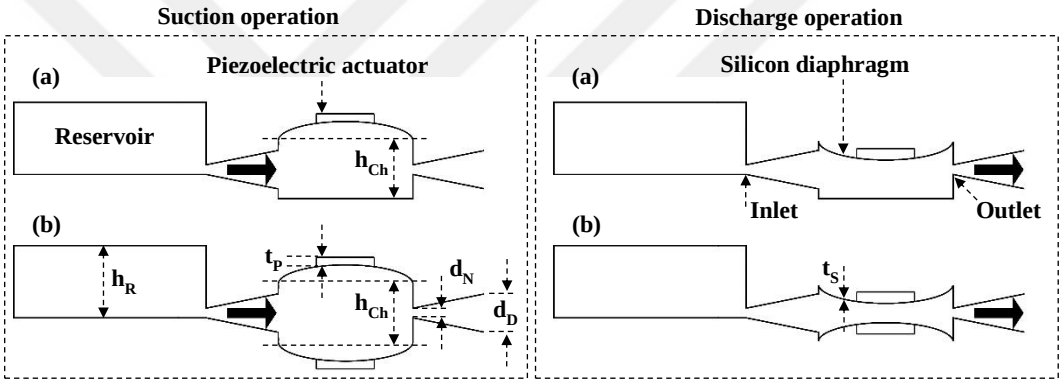

Figure 3.3. The working principle of the proposed micro-pumps, (a) SDM, (b) BDM

3.2. Displacement Analysis of Multi-Layer Piezoelectric Actuator

In this study, under the uniform fluid pressure and voltage load, the static displacement of the multi-layer circular actuator that contain silicon at the bottom, the passive structure made of brass at the center, and the active PZT on the top is investigated analytically, numerically and experimentally. The multi-layer actuator model is composed of three main layers in different radii with silicon, brass and PZT, and of four interlayers with silver and adhesive. In the modeling studies, classical multi-layer plaque theory based on Kirchhoff thin plate theory is used. The mathematical model, which is the solution of the static displacement equation of the non-homogenous multi-layer actuator of micro-pump, depends on the applied voltage and pressure load together with the material and physical properties. The electric-solid interaction of the

piezoelectric actuator and the silicon diaphragm (layer) under the effect of applied voltage load, and the silicon-fluid interaction under the uniform fluid pressure are simulated by modeling with finite elements. In addition, the maximum displacement of the multi-layer actuator with silicon exposed to flow and voltage load was measured experimentally. It was observed that the results obtained from analytical model, finite element analysis and experimental studies were sufficiently compatible with each other.

3.2.1. Static modeling of multi-layer actuator displacement

The structure of the multi-layer actuator was shown in Figure 3.4. The silicon, brass and PZT layers were connected by thin layers of adhesive. The effect of any layer was not neglected. The displacement caused by the voltage load applied to the PZT layer is amplified and transmitted to the silicon layer, which is the elastic layer, and then to the fluid, so that the fluid moves from the inlet to the outlet. Silicon, which was the elastic layer of the multi-layer actuator, was exposed to built-in boundary conditions throughout its circumference. The circular coordinate system was selected for analytical modeling of a multi-layer actuator with a circular geometry.

The classical laminated plate theory (CLPT) based on Kirchhoff's thin plate theory was used to obtain closed form displacement solutions and to analytically model the multi-layer circular actuator structure subjected to fluid pressure and voltage load. Accordingly, for lateral and transverse deviations of a multi-layered axial symmetry laminated actuator the general solution was obtained by the classical laminated plate theory. This multi-layer actuator consists of a uniform thickness of silicon, brass and PZT layers with "R_i", "R_m" and "R_o" radii respectively. The closed form of transverse displacement of the bottom silicon layer forming the multi-layer actuator was found by the general solution. According to CLPT, all multi-layer actuator layers were perfectly connected to each other.

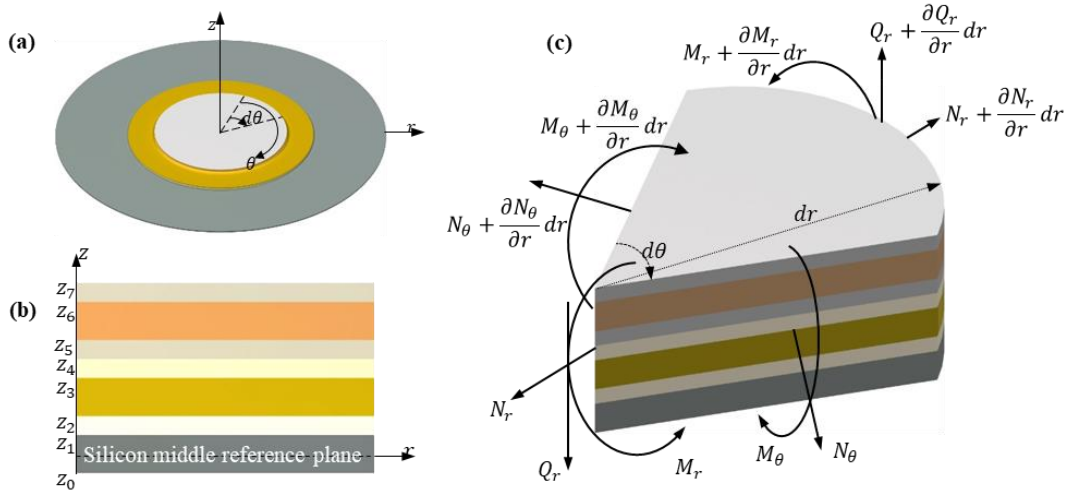

Figure 3.4. The structure of the multi-layer actuator, (a) the circular coordinate system, (b) physical layer structures, (c) the forces and moments of the diaphragm volume element

The material of each layer was isotropic and obeyed the Hook's law. The thicknesses of the layers were uniform. The strain and displacements were very small and plane strain conditions were valid. The transverse shear forces on the top and bottom surfaces of each layer were close to zero. In addition, PZT coefficients were assumed to be isotropic ($d_{31} = d_{32}$). In Kirchhoff's thin plate theory, "σ_r", "σ_θ" and "τ_{rz}" are axial stresses for small displacements. "σ_r" and "σ_θ" are the normal stresses in radial and angular directions, "τ_{rz}" indicates the shear stress from the "r" radial direction to "z" the normal direction.

Kinematic relations of identical layers of equal radii were defined in circular polar coordinates. The mid-plane of the silicon layer at the bottom of the piezoelectric actuator was selected as the reference plane. The z-axis was selected as the vertical axis. Each multi-layer actuator layer is sequentially located as i = 1, 2…, n from the lowest silicon layer. The bottom surface of the silicon layer was the z_0 plane and the upper surface of each layer was the z_i plane. Thus, the thickness of each layer was $h_i = z_i - z_{i-1}$.

According to Kirchhoff's thin plate theory for polar coordinates, the radial (ε_{rr}) and circumferential strain ($\varepsilon_{\theta\theta}$) relations of all points on the mid-plane of the reference silicon plane are as follows.

$$\varepsilon_{rr} = \frac{\partial u_r}{\partial r} \tag{3.1}$$

$$\varepsilon_{\theta\theta} = \frac{u_r}{r} \tag{3.2}$$

Here, the radial (u_r) and lateral (u_θ) displacements of the reference plane are given as;

$$u_r = -z\frac{\partial w}{\partial r} \tag{3.3}$$

$$u_\theta = -\frac{z}{r}\frac{\partial w}{\partial r} \tag{3.4}$$

where, "w" is the transverse displacement of the reference plane in the vertical (z) direction; and "θ" is the transverse slope. With the help of radial (u_r) and lateral (u_θ) displacement expressions, the radial and circumferential (lateral) strain relations for the displacement of the reference plane are as follows.

$$\varepsilon_r = \frac{\partial u_r}{\partial r} = -z\frac{\partial^2 w}{\partial r^2} \tag{3.5}$$

$$\varepsilon_\theta = \frac{u_r}{r} = -\frac{z}{r}\frac{\partial w}{\partial r} \tag{3.6}$$

The PZT layer of the multi-layer actuator was polarized along the vertical z-axis through its thickness. It was assumed that the electric field applied to the PZT layer of the actuator was homogeneous throughout the layer thickness.

$$\varepsilon_1 = s_{11}^E \sigma_1 + E_3 d_{31} \tag{3.7}$$

$$s_{11}^E = 1/E_p \tag{3.8}$$

where, "s_{11}^E" is the elastic compliance constant, "E_p" is Young's modulus of the PZT layer, "d_{31}" is PZT constant, "E_3" is the electric field strength along the vertical z-axis and changes to "$E_3 = V / t_{pzt}$" depending on the applied voltage load. According to the

thin plate theory, in the case of axisymmetric displacement, small in-plane shear components can be negligible. Assuming a linear strain distribution along with the multi-layer actuator layers, the strain constitutive equations for any layer will be similar to Equation 3.9.

$$\begin{Bmatrix} S_r \\ S_\theta \end{Bmatrix} = \begin{Bmatrix} \frac{\partial u_r}{\partial r} - E_3 d_{31} \\ \frac{u_r}{r} - E_3 d_{31} \end{Bmatrix} - z \begin{Bmatrix} \frac{\partial^2 w}{\partial r^2} \\ \frac{1}{r}\frac{\partial w}{\partial r} \end{Bmatrix} \tag{3.9}$$

Hence continuity equations for radial and circumferential stress will be as in Equation 3.10.

$$\begin{Bmatrix} \sigma_r \\ \sigma_\theta \end{Bmatrix} = \frac{E}{1-\mu^2} \begin{bmatrix} 1 & \mu \\ \mu & 1 \end{bmatrix} \begin{Bmatrix} S_r \\ S_\theta \end{Bmatrix} \tag{3.10}$$

where “E” is the Young’s modulus of the respective layer and “μ” is the Poisson's ratio of the respective layer. The Poisson's ratio is “$\mu = -s_{12}^E \,/\, s_{11}^E$” for the PZT layer. The radial and circumferential force resultants, “N_r” and “N_θ” are;

$$\begin{Bmatrix} N_r \\ N_\theta \end{Bmatrix} = D_1 \begin{Bmatrix} \frac{\partial u_r}{\partial r} - E_3 d_{31} \\ \frac{u_r}{r} - E_3 d_{31} \end{Bmatrix} - D_2 \begin{Bmatrix} \frac{\partial^2 w}{\partial r^2} \\ \frac{1}{r}\frac{\partial w}{\partial r} \end{Bmatrix} \tag{3.11}$$

The bending moments per unit length, “M_r” and “M_θ”, are radial and circumferential directions are;

$$\begin{Bmatrix} M_r \\ M_\theta \end{Bmatrix} = D_2 \begin{Bmatrix} \frac{\partial u_r}{\partial r} - E_3 d_{31} \\ \frac{u_r}{r} - E_3 d_{31} \end{Bmatrix} - D_3 \begin{Bmatrix} \frac{\partial^2 w}{\partial r^2} \\ \frac{1}{r}\frac{\partial w}{\partial r} \end{Bmatrix} \tag{3.12}$$

Here, the bending stiffness matrix of the circular plate “D_1”, “D_2” and “D_3” are as follows.

$$D_1 = \sum_{i=1}^{n} \int_{z_{i-1}}^{z_i} \frac{E_i}{1-\mu_i^2} \begin{bmatrix} 1 & \mu_i \\ \mu_i & 1 \end{bmatrix} dz \tag{3.13}$$

$$D_2 = \sum_{i=1}^{n} \int_{z_{i-1}}^{z_i} \frac{E_i z}{1-\mu_i^2} \begin{bmatrix} 1 & \mu_i \\ \mu_i & 1 \end{bmatrix} dz \tag{3.14}$$

$$D_3 = \sum_{i=1}^{n} \int_{z_{i-1}}^{z_i} \frac{E_i z^2}{1-\mu_i^2} \begin{bmatrix} 1 & \mu_i \\ \mu_i & 1 \end{bmatrix} dz \tag{3.15}$$

Equations of equilibrium in terms of the multi-layer piezoelectric actuator force, depending on the constant pressure "P", are as follows.

$$\frac{dN_r}{dr} + \frac{N_r - N_\theta}{r} = 0 \tag{3.16}$$

$$\frac{dQ_r}{dr} + \frac{Q_r}{r} + P = 0 \tag{3.17}$$

Here, N_r and N_θ are radial and tangential normal forces. "Q_r" is the vertical shear force in the Equation 3.18.

$$Q_r = \frac{dM_r}{dr} + \frac{M_r - M_\theta}{r} \tag{3.18}$$

The new equations are obtained by replacing the Equation 3.11 and Equation 3.12 in the Equation 3.16 and Equation 3.18, respectively.

$$D_{11}\left\{\frac{\partial^2 u_r}{\partial r^2} + \frac{1}{r}\frac{\partial u_r}{\partial r} - \frac{u_r}{r^2}\right\} - D_{21}\left\{\frac{\partial^3 w}{\partial r^3} + \frac{1}{r}\frac{\partial^2 w}{\partial r^2} - \frac{1}{r^2}\frac{\partial w}{\partial r}\right\} = 0 \tag{3.19}$$

$$D_{21}\left\{\frac{\partial^2 u_r}{\partial r^2} + \frac{1}{r}\frac{\partial u_r}{\partial r} - \frac{u_r}{r^2}\right\} - D_{31}\left\{\frac{\partial^3 w}{\partial r^3} + \frac{1}{r}\frac{\partial^2 w}{\partial r^2} - \frac{1}{r^2}\frac{\partial w}{\partial r}\right\} = Q_r \tag{3.20}$$

Here, "D_{11}", "D_{21}" and "D_{31}" are as follows.

$$D_{11} = \sum_{i=1}^{n} \frac{E_i(z_i - z_{i-1})}{1-\mu_i^2} \tag{3.21}$$

$$D_{21} = \sum_{i=1}^{n} \frac{E_i(z_i^2 - z_{i-1}^2)}{2(1-\mu_i^2)} \tag{3.22}$$

$$D_{31} = \sum_{i=1}^{n} \frac{E_i(z_i^3 - z_{i-1}^3)}{3(1-\mu_i^2)} \tag{3.23}$$

By evaluating Equation 3.19 and Equation 3.20 together, Equation 3.24 and Equation 3.25 are given as follows.

$$\frac{\partial^4 w}{\partial r^4} + \frac{2}{r}\frac{\partial^3 w}{\partial r^3} - \frac{1}{r^2}\frac{\partial^2 w}{\partial r^2} + \frac{1}{r^3}\frac{\partial w}{\partial r} = K_1 P \tag{3.24}$$

$$\frac{\partial^2 u_r}{\partial r^2} + \frac{1}{r}\frac{\partial u_r}{\partial r} - \frac{u_r}{r^2} = \frac{4}{r}K_3 C_3 + \frac{K_2 P r}{2} \tag{3.25}$$

"K_1", "K_2" and "K_3" are physical stiffness parameters and they are given in Equation 3.26, Equation 3.27 and Equation 3.28, respectively.

$$K_1 = \frac{D_{11}}{D_{11}D_{31} - D_{21}^2} \tag{3.26}$$

$$K_2 = \frac{D_{21}}{D_{11}D_{31} - D_{21}^2} \tag{3.27}$$

$$K_3 = \frac{D_{21}}{D_{11}} \tag{3.28}$$

Equation 3.24 shows the transverse movement of all points of the multi-layer actuator. This equation is non-homogeneous fourth order linear ordinary differential equation. Equation 3.25 is a non-homogeneous second order linear ordinary differential equation that shows the lateral movement of all points of the multi-layer actuator. The transverse and lateral general solution of the multi-layer actuator can be found as in Equation 3.29 and Equation 3.30.

$$w(r) = C_1 r^2 + C_2 \ln r + C_3 r^2 \ln r + C_4 + \frac{K_1 P}{64} r^4 \tag{3.29}$$

$$u(r) = C_3K_3(2\ln r - 1)r + C_5r + C_6\frac{1}{r} + \frac{K_2P}{16}r^3 \quad (3.30)$$

where "C_1", "C_2", "C_3", "C_4", "C_5" and "C_6" are the integration constants obtained from the boundary conditions. Note that the solutions obtained are not a function of voltage. However, the constants "C_1", "C_2", "C_3", "C_4", "C_5" and "C_6" contain physical parameters such as material properties, as well as the voltage function applied to the PZT layer. Therefore, after applying the boundary conditions, the voltage parameter will also appear in the equations. Silicon diaphragm was fully clamped on to the chamber (see Figure 3.5.). To obtain the transverse displacement of a partially covered and seven-layer actuator, the structure was divided into three steps: exterior annulus ($R_m \leq r \leq R_o$), the middle annulus ($R_i \leq r \leq R_m$) and interior core ($0 \leq r \leq R_i$) (see Figure 3.6.).

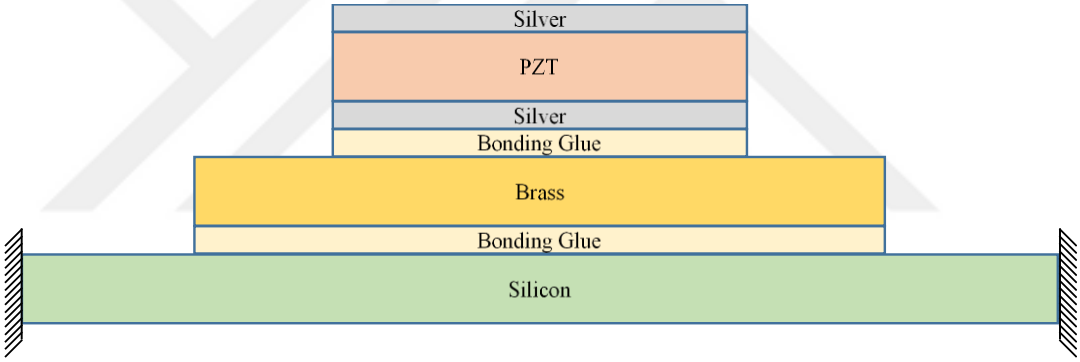

Figure 3.5. Cross-sectional schematic view of the multi-layer actuator

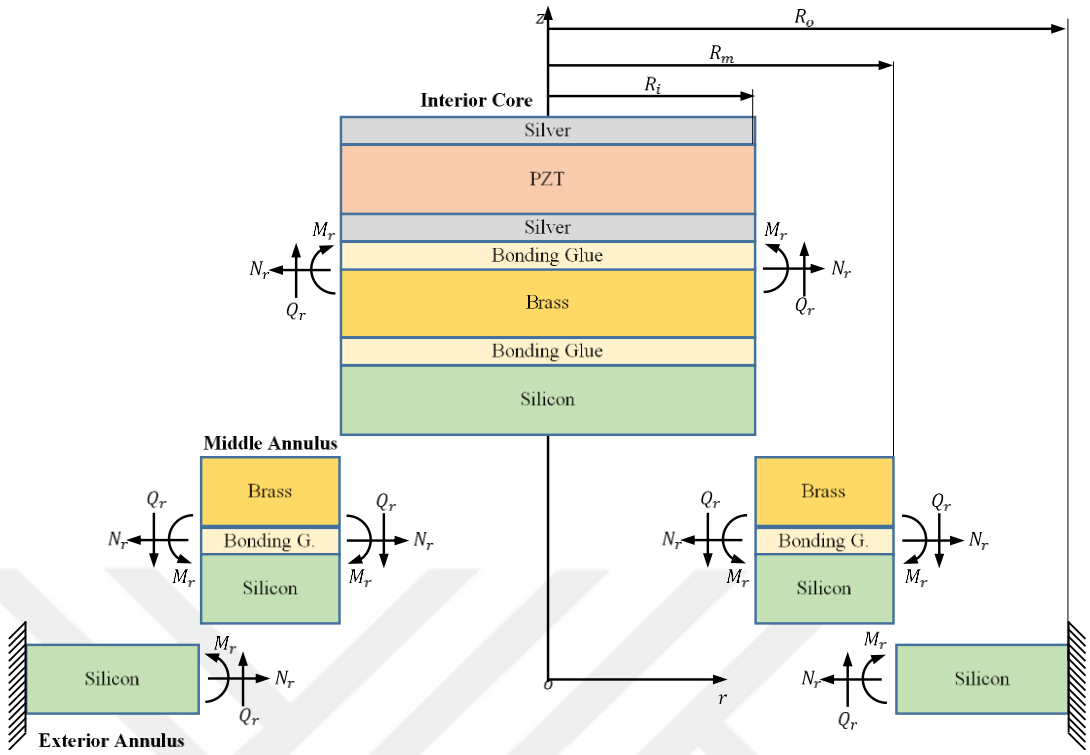

Figure 3.6. Convention for coordinate frame and the positive directions of the forces and moments

With the help of Equations 3.29 and Equations 3.30, the transverse and lateral displacements for the actuator layer were rearranged from the Equations 3.31 to Equation 3.36.

$$w_{ext}(r) = C_1 r^2 + C_2 \ln r + C_3 r^2 \ln r + C_4 + \frac{K_1^{ext} P}{64} r^4 \qquad R_i \le r \le R_m \qquad (3.31)$$

$$w_{mid}(r) = C_7 r^2 + C_8 \ln r + C_9 r^2 \ln r + C_{10} + \frac{K_1^{mid} P}{64} r^4 \qquad R_i \le r \le R_m \qquad (3.32)$$

$$w_{int}(r) = \frac{K_1^{int} P}{64} r^4 + C_{13} r^2 + C_{14} \ln r + C_{15} r^2 \ln r + C_{16} \qquad 0 \le r \le R_i \qquad (3.33)$$

$$u_{ext}(r) = C_3 K_3^{ext} r(2 \ln r - 1) + C_5 r + C_6 + \frac{K_2^{ext} P}{16} r^3 \qquad R_i \le r \le R_m \qquad (3.34)$$

$$u_{mid}(r) = C_9 K_3^{mid} r(2 \ln r - 1) + C_{11} r + C_{12} + \frac{K_2^{mid} P}{16} r^3 \qquad R_i \le r \le R_m \qquad (3.35)$$

$$u_{int}(r) = \frac{K_2^{int} Pr^3}{16} + C_{15} K_3^{int} r(2\ln r - 1) + C_{17} r + C_{18} \frac{1}{r} \quad 0 \le r \le R_i \tag{3.36}$$

Here, "w_{ext}", "w_{mid}", "w_{int}" were transverse displacements solutions of external area, middle area, and center (internal) area, respectively. "u_{ext}", "u_{mid}", "u_{int}" were lateral displacements solutions of external area, middle area and center (internal) area, respectively. Provided that according to Hooke's law the displacement of the center point of the actuator structure (r = 0), accepted to operate in the elastic region is limited, it is required "C_{14}", "C_{15}" and "C_{18}" to be zero in Equation (3.33) and Equation (3.36). ($C_{14} = C_{15} = C_{18} = 0$). The boundary conditions of the multi-layer actuator components are given from Equation (3.37) to Equation (3.51). By applying these boundary conditions in transverse displacement Equations of (3.31), (3.32) and (3.33), other coefficients "C_1", "C_2", ...can easily be found. In the later stages of the study, only transverse displacements are considered, rather than lateral displacements.

Boundary conditions on the outer plate at $r = R_o$

$$w_{ext}(R_o) = 0 \tag{3.37}$$

$$\partial w_{ext}(R_o)/\partial r = 0 \tag{3.38}$$

$$u_{ext}(R_o) = 0 \tag{3.39}$$

The continuity and equilibrium conditions at $r = R_m$

$$w_{ext}(R_m) = w_{mid}(R_m) \tag{3.40}$$

$$\partial w_{ext}(R_m)/\partial r = \partial w_{mid}(R_m)/\partial r \tag{3.41}$$

$$u_{ext}(R_m) = u_{mid}(R_m) \tag{3.42}$$

$$N_r^{ext}(R_m) = N_r^{mid}(R_m) \tag{3.43}$$

$$M_r^{ext}(R_m) = M_r^{mid}(R_m) \tag{3.44}$$

$$Q_r^{ext}(R_m) = Q_r^{mid}(R_m) \tag{3.45}$$

The continuity and equilibrium conditions at $r = R_i$

$$w_{mid}(R_i) = w_{int}(R_i) \tag{3.46}$$

$$\partial w_{mid}(R_i)/\partial r = \partial w_{int}(R_i)/\partial r \tag{3.47}$$

$$u_{mid}(R_i) = u_{int}(R_i) \tag{3.48}$$

$$N_r^{mid}(R_i) = N_r^{int}(R_i) \tag{3.49}$$

$$M_r^{mid}(R_i) = M_r^{int}(R_i) \tag{3.50}$$

$$Q_r^{mid}(R_i) = Q_r^{int}(R_i) \tag{3.51}$$

The analytical solutions of the seven-layer and partially covered piezoelectric actuator in closed form can help to determine the static displacement behavior under constant voltage and fluid pressure. The physical parameters used to obtain the static displacement behavior of the multi-layer piezoelectric actuator were given in Table 3.2. The physical properties of PZT were given in Table 3.3.

Table 3.2. Physical properties of multi-layer piezoelectric actuator

Layer	Silicon	Bonding Glue (b)	Brass	Bonding Glue (t)	Silver	PZT
Radius (mm)	12.5	7	7	5	5	5
Thickness (μm)	100	10	100	10	10	100
Young's modulus (GPa)	162	5.17	110	5.17	40	63
Poisson ratio	0.22	0.3	0.27	0.3	0.35	0.3
Piezoelectric coefficient d_{31} (C/N)	-	-	-	-	-	1.75×10^{-10}

Table 3.3. Physical property of piezoelectric actuator (PZT-2)

Property	Tensor (in order of x, y, z, xy, yz and xz)
PZT stress tensor e (C/m^2)	$\begin{bmatrix} 0 & 0 & -1.81603 \\ 0 & 0 & -1.81603 \\ 0 & 0 & 9.05058 \\ 0 & 9.77778 & 0 \\ 9.77778 & 0 & 0 \\ 0 & 0 & 0 \end{bmatrix}$
Elastic matrix C^E (N/m^2)	$\begin{bmatrix} 13.48 & 6.78 & 13.48 & 0 & 0 & 0 \\ 6.80 & 6.80 & 11.32 & 0 & 0 & 0 \\ 0 & 0 & 0 & 0 & 0 & 0 \\ 0 & 0 & 0 & 2.22 & 0 & 0 \\ 0 & 0 & 0 & 0 & 2.22 & 0 \\ 0 & 0 & 0 & 0 & 0 & 3.34 \end{bmatrix}$
Compliance matrix (1/Pa)	$\begin{bmatrix} 11.6 & -3.33 & 11.6 & 0 & 0 & 0 \\ -4.97 & -4.97 & 1.48 & 0 & 0 & 0 \\ 0 & 0 & 0 & 0 & 0 & 0 \\ 0 & 0 & 0 & 45 & 0 & 0 \\ 0 & 0 & 0 & 0 & 45 & 0 \\ 0 & 0 & 0 & 0 & 0 & 29.9 \end{bmatrix}$
Relative permittivity (F/m)	$\begin{bmatrix} 504.1 & 0 & 0 \\ 0 & 504.1 & 0 \\ 0 & 0 & 270 \end{bmatrix}$

3.2.2. Finite element analysis

In this study, the mesh convergence method was used to obtain satisfactory displacement amplitude of the diaphragm where the values saturated. According to the results, the displacement reached maximum at the center and zero at the edges. Clearly, diaphragm in supply mode showed more displacement than pump mode. In contrast, we examined the diaphragm displacement in pump mode, because the diaphragm applied maximum force to the fluid in this period. The analysis was done when the excitation input was at 5 V and 5 Hz to the piezoelectric actuator. The analysis consists of four steps in the COMSOL Multiphysics 4.3 program. The four different types of meshes were selected. The number of meshes used in first step was less than the second step and this was repeated until the fourth step. The properties of the mesh were given in Table 3.4.

Table 3.4. Specifications of Finite Element Method (FEM)

Domain element statistics		Number of elements	Minimum element quality	Average element quality	Element area ratio	Maximum growth rate	Average growth rate
SDM	Normal	9976	0.08694	0.8535	0.01245	3.521	1.34
	Fine	16832	0.1255	0.8758	0.02373	3.547	1.256
	Finer	44268	0.1262	0.9006	0.00727	3.481	1.264
	Ext. Fine	113730	0.1262	0.9196	0.00349	3.487	1.233
BDM	Normal	9767	0.1254	0.8505	0.01259	3.588	1.348
	Fine	15786	0.1272	0.8645	0.01951	3.519	1.257
	Finer	42861	0.1262	0.9013	0.00932	3.5	1.265
	Ext. Fine	113635	0.1262	0.9231	0.00351	3.492	1.229

The error rates between the first meshing step (Normal) and the second meshing step (Fine) for the diaphragm displacement of SDM and BDM were 3.25 %, and 8.29 %, respectively. For these micro-pumps, the values were the very close at the second and subsequent steps. In the mesh convergence method, if the number of mesh elements is high, this increases the accuracy of the results. However, the analysis time will be highly increased. Therefore, we used the second step (Fine) mesh for the diaphragm displacement analysis. The displacement results were given in Chapter 4.

3.2.3. Experimental analysis of diaphragm displacement

The diaphragm displacement was experimentally measured with a Fotonic Sensor (MTI-2100, MTI Instruments, Albany, NY, USA). It is a Fiber-optic non-contract sensor that uses reflection electronic technologies to accurately measure of diaphragm displacement. It is worth mentioning that the diaphragm displacement depends on the geometry and material properties of the multi-layer piezoelectric actuator. In this study, the diaphragm displacement was measured with a sensitivity of 0.01 μin. The experimental diaphragm displacement measurement setup was shown in Figure 3.7. However, the results of the experimental measurements of the diaphragm displacement were shown in Chapter 4.

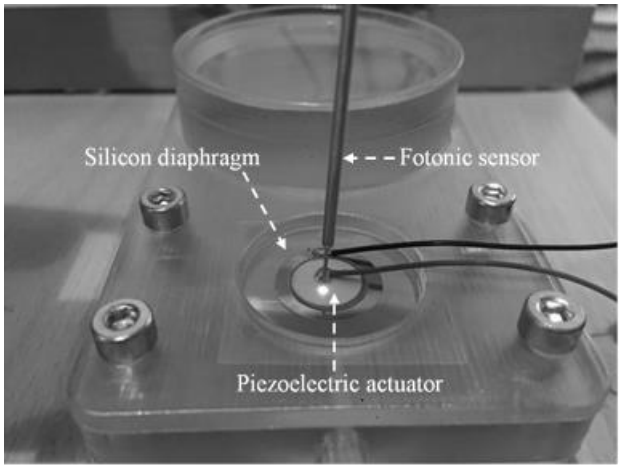

Figure 3.7. Experimental measurement setup of diaphragm displacement

3.3. Micro-pump Calibration and Flow Test

In this study micro-pumps and fluid reservoir were fabricated as adjacent as shown in Figure 3.8. Each micro-pump (SDM and BDM) had a fluid reservoir. The micro-pump chamber was connected with reservoir through a nozzle/diffuser element. The nozzle/diffuser elements did not have moving components. Therefore, when the voltage was not applied to the piezoelectric (inactive status), always a constant amount of flow rate was obtained due to water height in reservoir. Therefore, hydrostatic pressure gradient occurred from reservoir (pointed as 1 in Figure 3.8) to outlet (2) of micro-pump and head loss caused by a sudden increase or decrease could be considered in theoretical calculation.

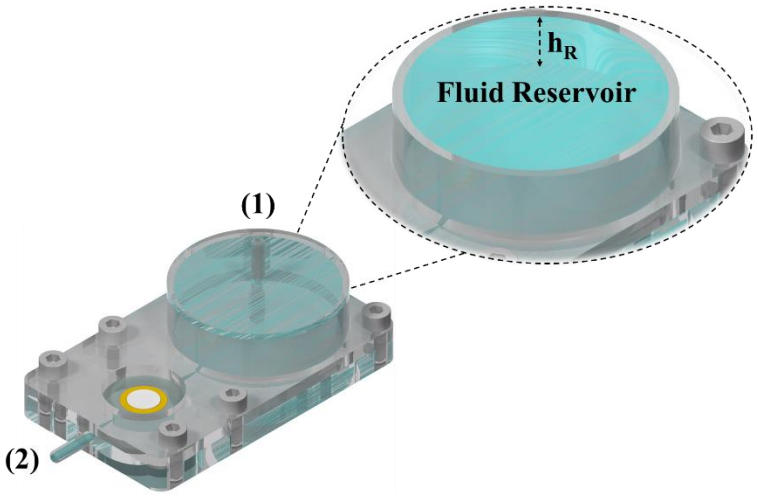

Figure 3.8. The effect of reservoir height on flow rate

While energy equation was applied for the one-dimensional control volume for not pumping, extended Bernoulli equation is expressed in Equation 3.52;

$$\frac{P_1}{\rho g} + \frac{v_1^2}{2g} + z_1 = \frac{P_2}{\rho g} + \frac{v_2^2}{2g} + z_2 + \Delta h_{total} \quad (3.52)$$

P: Fluid pressure, v: Fluid Velocity, z: Height of streamline, ρ: Fluid density, g: Gravity constant. "P_1" and "P_2" are atmospheric pressures, "v_1" and "z_2" are equal to zero. Finally, "Δh_{total}" total head loss is consisted of friction (f) and minor losses,

$$\Delta h_{total} = \left(f \frac{L}{D} + \sum K\right) \frac{v^2}{2g} \quad (3.53)$$

where, "L" is the length, "D" is the diameter and "K" is the loss coefficient. In the literature, values of "K" have been studied for nozzle and diffusers [171, 172]. Based on literature studies, total head loss was obtained with Equation 3.53. Additionally, the theoretical flow rates were calculated according to the liquid height in the reservoir. Then theoretical flow rates are confirmed by the experimental data collected on inactive status. In order to determine the flow rates caused only by piezoelectric actuator, the experiments were repeated while the piezoelectric actuator on active status. The flow tests for SDM and BDM micro-pumps were performed on active and inactive status and actual piezoelectric actuator flow rates were determined subtracting from each other.

Water has been used as a working fluid in the investigation. In experiments, the fluid (water) was at ambient conditions (20.0 – 21.0 ^oC). Mass flow measurement has been done by both from precision glass syringe and measuring water weight collected on a digital balance (Mettler Toledo ML200T). All the measurements were repeated at least three times to improve reliability of the flow tests. The analyzed measurement uncertainties were calculated according to the method presented by Kline and McClintock [173]. Standard deviation of flow rates was calculated and random errors were determined by multiplying by 1.95 for 95% confidence level. Standard uncertainties of measured parameters were: 21 ^oC ±0.6 for inlet temperature; 60 s

±0.0003 for time interval; 10 g ±0.01 for digital balance and 999 kg/m^3 ±0.1 for density of water. As a result, the highest uncertainties of volume and mass flow rate were calculated for tests under conducted 5 V and 5 Hz as ∓ 2.2 % and ∓ 2.3 % respectively.

CHAPTER 4. RESULTS AND DISCUSSIONS

The purpose of this chapter was to provide a general result of the proposed study. In this chapter, the results and achievements of the study have been interpreted specifically. Additionally, some of the previous studies related to the subject of this thesis are presented in this chapter. The results obtained of the presented micro-pumps in this thesis are compared and analyzed with those reported in the previous studies. Moreover, the advantages and disadvantages of the current study have been carefully investigated with previous studies.

4.1. Drop Shape Analysis (DSA)

Surface roughness, porosity and hydrophilicity are important factors in fluid mechanics because they can affect interactions between fluid and solid. The nozzle /diffuser elements, the chamber and the fluid reservoir were fabricated from PMMA. Drop shape analysis (DSA) was performed to determine the contact angle from the shadow image of a sessile drop and the surface tension or interfacial tension from the shadow image of a pendant drop. Drop shape analysis (DSA) was performed by KRÜSS (DSA100M, KRÜSS GmbH, Germany) measuring instruments with a sensitivity of 0.05˚. This test was repeated 3 times at 20˚C. The average of performed analysis of contact angle showed that a drop water was 58.36˚ (±2.85˚). The results showed that the PMMA used in this study was hydrophilic and usual no-slip boundary condition was still valid. In other words, there is no self-filling and fluid flow due to the hydrophilic properties in flow tests. The DSA results are shown in Figure 4.1.

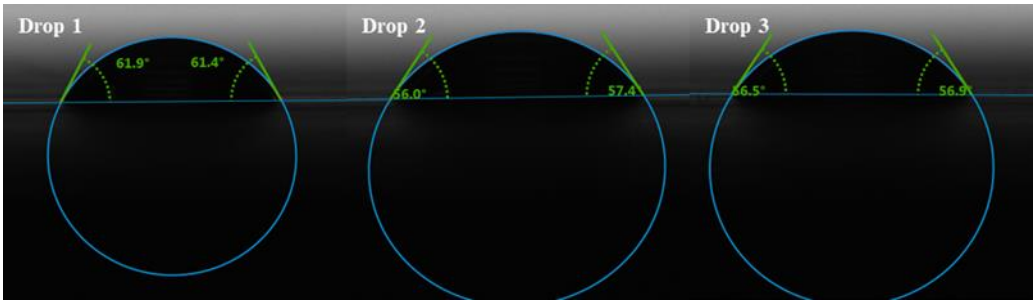

Figure 4.1. Drop shape analysis for PMMA material

4.2. Microscopic Image Investigation

Microscopic images were used to evaluate surface properties of micro-pump due to the possibility of testing with biological fluids in the future studies. As described in Chapter 3, the nozzle/diffuser elements, the chamber and the fluid reservoir were fabricated in clean room by the rapid prototyping device (Objet260 Connex3) with 16-micron layer resolution. Therefore, we examined a piece of the PMMA material in the field-emission scanning electron microscope (FSEM). Moreover, profilometer was used to visualize surface porosity and roughness characteristics of PMMA surface. In most cases, porosity and roughness are undesirable while, depending on the type of application, pore structures on the flow surface are preferred.

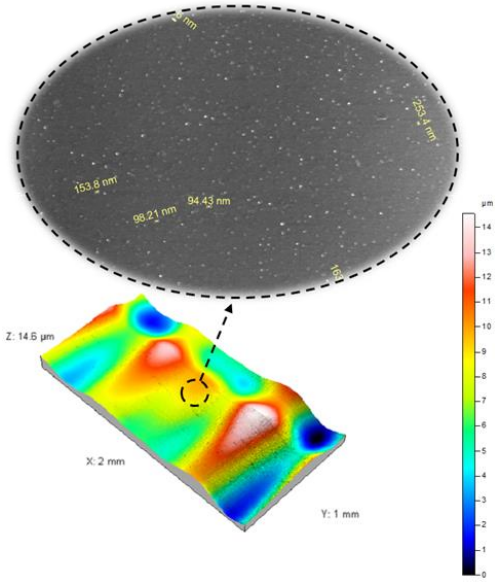

Figure 4.2. FSEM and Profilometer image of PMMA for porosity and roughness measurements

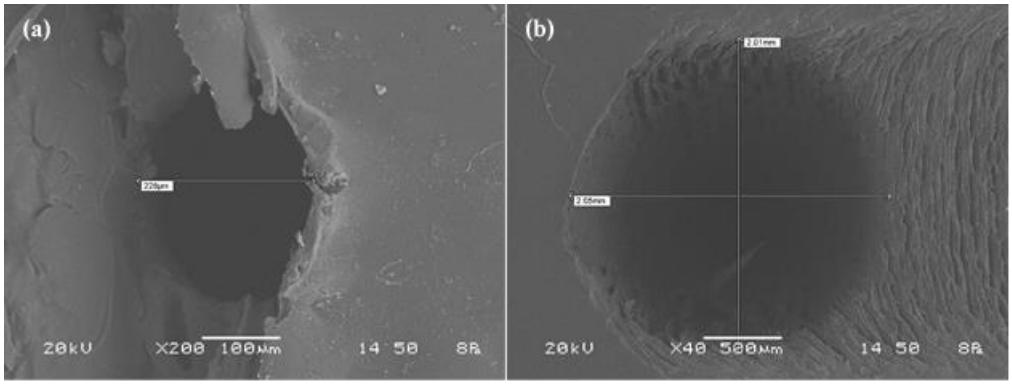

Figure 4.3. A (SEM) images of PMMA (a) Nozzle/ diffuser inlet (b) Nozzle/ diffuser outlet

As shown in Figure 4.2., undesired porosity was in the nanometer size, flow surface was completely assumed as smooth surface. In addition, the mean roughness was measured as 383.4 Å. Thereby, the undesired particles and the amount of the roughness of the PMMA surface have no effect on the fluid behavior of the chamber or the fluid in the nozzle/diffuser elements. Another important issue was to determine the inlet and outlet diameters of the nozzle/diffuser elements in terms of the reliability of the calibration. Hydraulic diameters were designed as 0.2 mm and 2 mm, and SEM was used to determine the exact sizes after fabrication. Figure 4.3. shows the image of the Scanning Electron Microscope (SEM) of (a) water inlet and (b) outlet sections to these nozzle/diffuser elements. The water in the chamber is entered to the nozzle/ diffuser with a hydraulic diameter of 257.07 µm. Moreover, the diameter of nozzle/ diffuser element was 2061.91 µm at the moment of full water discharge. This causes at the discharge moment, the pressure to increase and the velocity to decrease.

4.3. Displacement Result of Circular Multi-Layer Piezoelectric Actuator

By FEM (Figure 4.4.a) and experimental studies (Figure 4.4.b), the accuracy of the analytical solutions (Figure 4.4.c) expressing the static displacement of the multi-layer micro-pump actuator was studied. In the analytical studies, the variation of displacement of the midpoint and all points on the midline under the influence of different voltage load (from 0 V to 45 V) and fluid pressure (from 0 Pa to 400 Pa) was investigated. Because, the diaphragm was exposed to these voltage and pressure values under real operating conditions. In all calculations, it was assumed the voltage load

and flow rate to be laminar in the micro-pump chamber and the fluid pressure to remain constant. The frequency was 0 Hz because of the static analysis. Whereas, in the FEM and experimental studies, frequencies were between 5 Hz and 20 Hz by 5 Hz steps. Static (DC) voltage load cannot be applied to piezo-elements. Because, the piezoelectric vertical vibration or displacement mode depends on the applied AC voltage which creates dynamic behavior. In order to compare the analytical solutions with the FEM and experimental results, we have considered the 5 Hz input voltage load. Because the 5Hz actuator frequency was relatively small, it was closer to the static displacement result. Figure 4.4.a shows the simulation results of diaphragm displacements at the moment of water discharge from the chamber. It shows that the increase in voltage increased displacement. Additionally, increasing the frequency reduced displacement in the range of 5-20 Hz. The displacement results have 99% liner behavior. The maximum displacement was obtained 4.097 μm in 45 V and 5 Hz.

Figure 4.4.b shows the experimental results of diaphragm displacements at the discharge operation. It shows that the displacement trends were similar with FEM results at all voltage and frequencies. The displacement results have 98% liner behavior. The maximum displacement was achieved 5.23 μm in 45 V and 5 Hz. Since diaphragm displacement was at micro-meter levels, measurement results were highly affected by environmental factors. The small differences might be because of the measurement errors, fluid movement noises in the micro-pump, mechanical vibrations from the experimental setup that cannot be controlled.

Analytical solutions were obtained considering static load to the multi-layer piezoelectric actuator (Figure 4.4.c). Fluid pressure and input frequency was assumed to be zero. Displacement behaviour was found to be 100% linear ($R^2 = 1$). External noises were neglected. Similarly, displacement values were increased as a function of voltage.

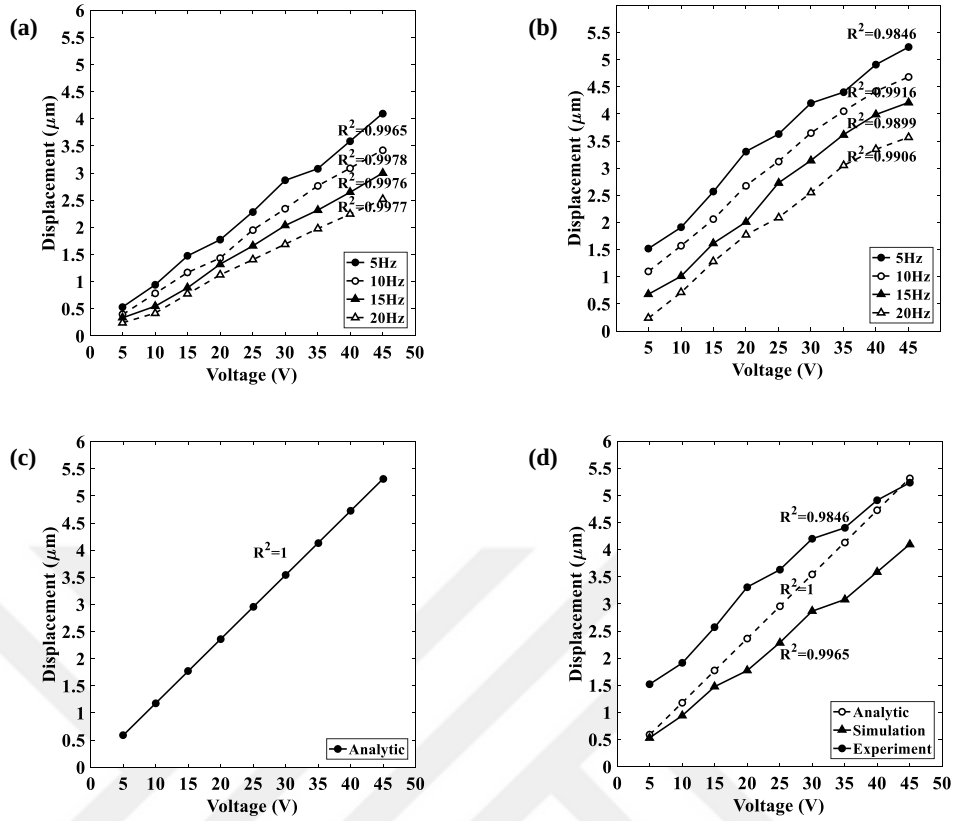

Figure 4.4. The mid-point displacement of the silicon diaphragm at 5 V-45 V for 0 Pa, (a) FEM, (b) experiment, (c) analytical, and (d) comparison of the displacement results

Hereby, the displacement of the midpoint of the silicon diaphragm was obtained by analytical, FEM and experimental methods as seen in Figure 4.4.d. It shows that the analytical, FEA and experimental results are very close and have similar trends. Due to the environmental conditions and the presence of environmental disturbances, slight differences have occurred in the experimental results related to FEM and analytical results.

While there was no fluid pressure, the displacement of the midline of the silicon layer at different voltages (0-45 V) was given in Figure 4.5.a. When the input voltage was zero, the displacement of the mid-line of the silicon layer under pressure loads of 0-400 Pa was given in Figure 4.5.b. As expected, the silicon layer remains completely horizontal in a completely unloaded state (0 Pa and 0 V). The displacement increases with increasing the voltage and pressure. The maximum displacement occurred at 45 V and it was 5.3146 μm at the mid-point of silicon diaphragm. The displacement of

the midline of the silicon layer at 5-45 V and the diaphragm exposed to 200 Pa constant fluid pressure load, was given in Figure 4.5.c. While the displacement up to 10 V electrical load is in positive direction, the displacement of the midline of the silicon for electric loads higher than 10 V increases in a negative direction. Note that the displacement of the exterior annulus portion of the diaphragm was less than that of the middle annulus and interior core portion.

The displacement of the midline of the silicon layer under fluid pressure of 0-400 Pa and 20 V constant voltage load was given in Figure 4.5.d. The interior displacement decreases as fluid pressure increases, and the middle core and exterior annulus displacement increase positively.

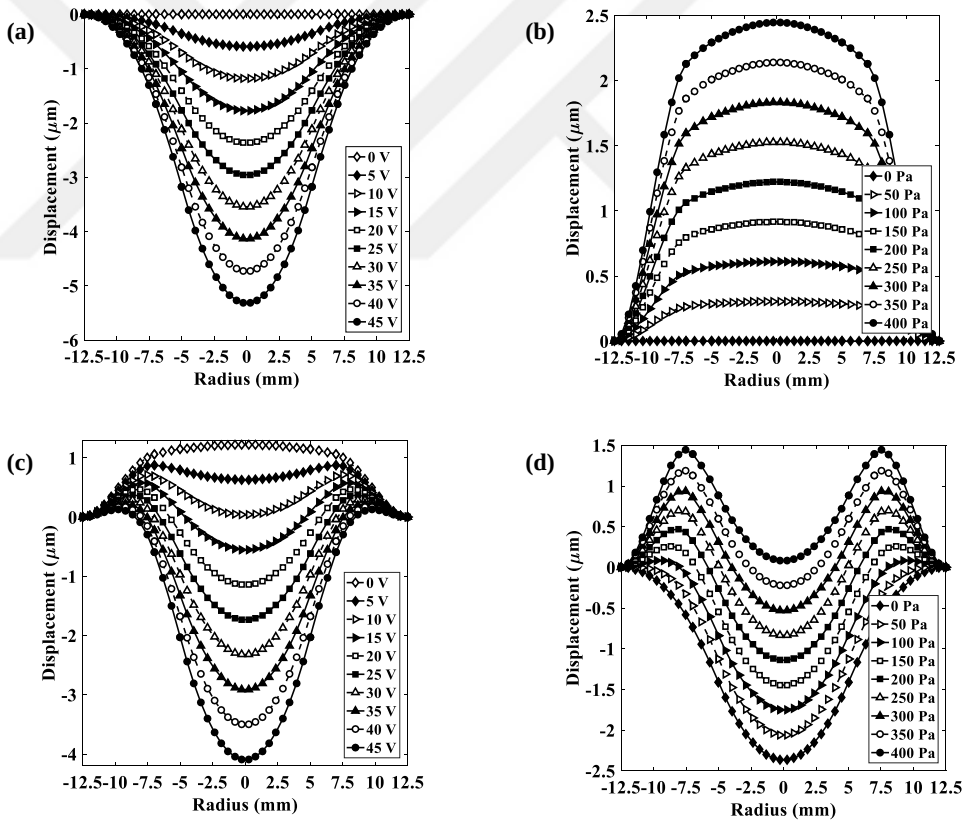

Figure 4.5. The displacements of the midline of the silicon layer at (a) 0-45 V for 0 Pa, (b) 0-400 Pa for 0 V, (c) 0-45 V for 200 Pa, and (d) 0-400 Pa for 20 V

The displacement of the mid-point of the silicon layer for different voltage and pressure loads were presented in Figure 4.6. As shown in both figures, the displacement of the midpoint changes linearly in all load conditions with increasing voltage or pressure. At a certain point, when the voltage and pressure loads are equal or very close to each other, the silicone layer remains fully horizontal and the midpoint displacement is zero. The minimum flow flow is obtained when the PZT voltage load and fluid pressure loads acting on the silicone layer are equal or close to each other. As the pressure load increases under constant voltage loads, firstly, the center-point displacement decreases up to reference plane. As the pressure continues to increase when the midpoint is in the horizontal position, the midpoint displacement starts to increase upwards in the positive direction. The PZT actuator cannot overcome the fluid pressure, so no pumping operation is performed. (see figure 4.6.a). As the voltage increases under constant pressure loads, firstly, the center-point displacement decreases up to reference plane and therefore the scuction mode is reduced. As the voltage continues to increase while the midpoint is in the horizontal position, the displacement of the midpoint starts to increase. As the ratio of the voltage load of the PZT actuator to the fluid pressure increases, the pumping operation begins to improve (see figure 4.6.b). The net flow rate values of the proposed micro-pumps were shown in Section 4.4. These results show that the most suitable values of the pressure and voltage loads should be selected for obtained maximum flow rate.

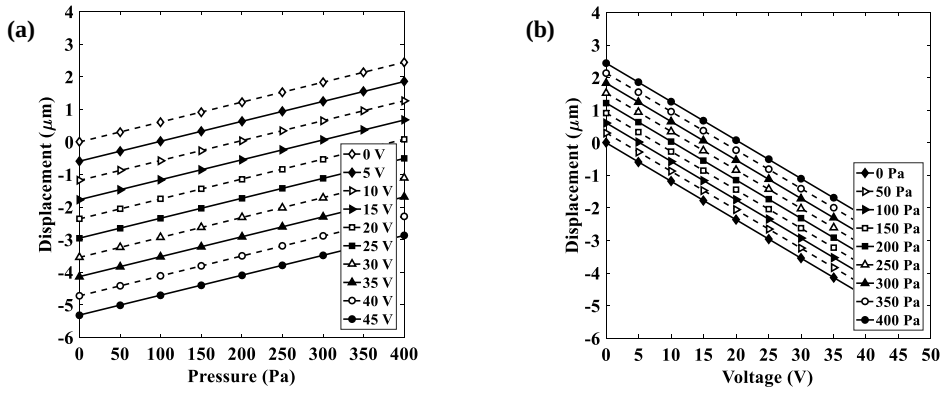

Figure 4.6. Mid-point displacements of the silicon diaphragm as a function of (a) pressure and (b) voltage

4.4. Experimental Results of the Flow Rates

At the mentioned voltages and frequencies, we measured the net flow rate of the micro-pumps. Figure 4.7 shows the results of flow rates of SDM and BDM micro-pumps. Voltage increment increased the flow rate. The frequency increase led to a decrease in displacement. However, due to the increase in the number of vibrations, the flow rate in both micro-pumps increased. The maximum flow rates obtained for SDM and BDM in 45 V and 20 Hz were 32.58 ml/min and 35.4 ml/min respectively.

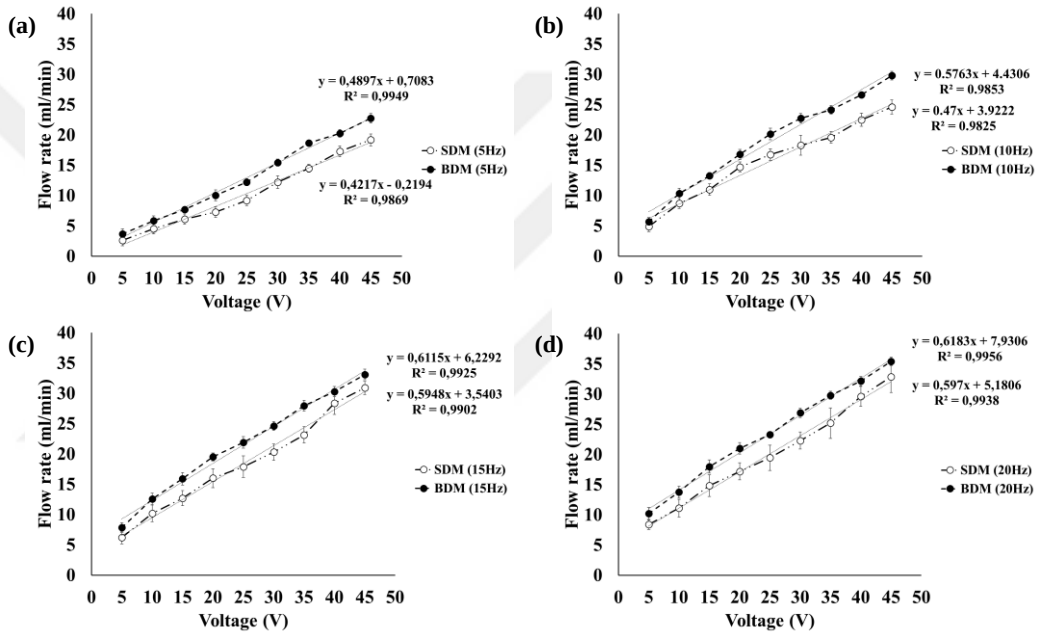

Figure 4.7. The maximum flow rate results at (a) 5 Hz, (b) 10 Hz, (c) 15 Hz and (d) 20 Hz

BDM consisted of a chamber sandwiched between two diaphragms actuated by two piezoelectric actuators at the same time to achieve high flow rate. Because, double actuator creates higher force to the fluid in the chamber compared to SDM having only single actuator. Thereby, the flow rate values were higher for BDM. Flow rates were increasing as a function of voltage according to our experimental results. The voltage determines the amplitude of the diaphragm vibration. Reverse piezoelectric effect causes the displacement changes as a function of applied voltage. There was linear correlation in Figure 4.7, linear behavior of each pump at different driving frequencies were given according to experimental measurement. At all frequencies, the slope of

the BDM was higher. So, with increasing voltage, the flow rates increase was higher compared to SDM.

The difference of flow rates (ΔQ: BDM-SDM) were calculated. For 5 Hz and 10 Hz, ΔQ is getting bigger with the voltage. It is an expected result because of the steeper slope of BDM equations at lower frequencies. When we increase the frequencies to 15 Hz and 20 Hz, the difference between slopes and also flow rates gets smaller. We plotted ΔQ as a function of voltage in Figure 4.8. The statistical analysis of flow rates showed that there was no significant flow rate difference between SDM and BDM when the voltage was increased (t-test, $p > 0.05$).

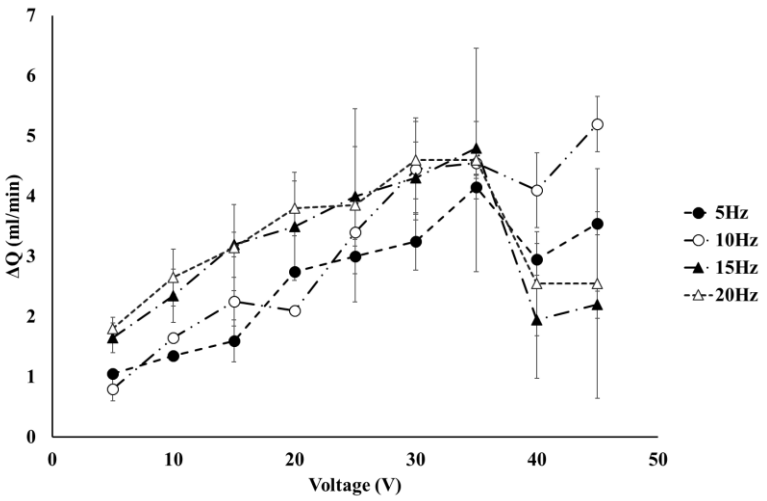

Figure 4.8. Flow rate difference (ΔQ: BDM-SDM)

4.5. Discussion

In this study, the performance of two novel micro-pumps was studied in the same experimental conditions. The only difference in the SDM and BDM was the number of vibrating diaphragms. Based on the results obtained in Section 4.4, the BDM flow rate compared to SDM at 5 Hz, 10 Hz, 15 Hz and 20 Hz were increased to 22%, 16.39%, 15.97% and 15.19% respectively. The water weight inside the chamber prevented moving the bottom diaphragm of the BDM. If the water weight force was not in the opposite direction of the bottom diaphragm force, we would expect a significant increase in the flow rate of the BDM design. As an important advantage, in

the daily usage BDM design gives an opportunity to use both side facing upwards without losing the flow rate when the reservoir is closed to the atmosphere and adjustable according to the nozzle elements.

4.5.1. Comparison with the state of the art

The flow rate of single chamber micro-pumps is limited due to the periodic displacement of the diaphragm. When the studies in Table 4.1 were investigated, it was seen that Afrasiab et al. (2011) and He et al. (2016) focused on increasing the limited flow rate of single chamber micro-pumps. Afrasiab et al. investigated the effects of a silicon diaphragm wave motion on the net flow rate by the finite element method. The upper ceiling wall of the chamber was covered with silicon diaphragm. Nine piezoelectric actuators were attached on the silicon diaphragm. The sinusoidal voltage was applied with $2\pi/3$ phase shift to piezoelectric actuators. Therefore, a peristaltic motion was applied to the fluid inside the chamber [174]. However, alternating pressures are the main factor of fluid motion. In their design, upper diaphragm was unable to apply pressure to the fluid in the bottom of the chamber. He et al. are focused on multi-chamber micro-pump. Consequently, their design created high flow rate compared to single chamber designs as expected [175]. However, in their multi-chamber design, there was a turbulence, which is not preferred in micro-pump designs. Kolahdouz et al. (2014) investigated the effects of different driving voltage shapes and frequencies on the diaphragm displacement and flow rate [176]. In their study, they used a glass diaphragm, which has the thickness of 300 μm. However, the thickness of piezoelectric actuator was 200 μm. Because of the stiffness of the glass material, relatively thin layer of piezoelectric actuator could not produce higher displacement values (~0.6 μm at 80 V). In our study, the displacement values of the diaphragm were almost 6 times higher (~3.6 in BDM) even though our driving voltage was 45 V. These results show the importance of the diaphragm and piezoelectric actuator thickness selection in the micro-pump designs.

The flow rate is a key parameter and can be controlled by the displacement of the diaphragm, whereas our proposed configuration (BDM) consist of a chamber

sandwiched between two diaphragms. Hereby, we have been able to apply an alternative pressure to the fluid below the chamber. Thus, we improved the net flow rate with a simple geometric correction by a different micro-pump design.

Sateesh et al. (2018) investigated the micro-channels diameter effects on flow velocity [177]. In the study, polydimethylsiloxane (PDMS) membrane with thickness of 20 μm was placed on top of the piezoelectric actuator. Furthermore, 20 μm thick ground electrode and active electrode were placed under the piezoelectric actuator. Thereby, the piezoelectric actuator was compressed between two layers. As a result, this compression increases the resistance to piezoelectric vibration. The low vibration amplitude of the piezoelectric actuator may have caused the pressure at this micro-pump to be low. However, when SDM is compared with this micro-pump, the thickness of the silicon diaphragm (100 μm) in the SDM was about half of the thickness of the piezoelectric actuator (200 μm). Therefore, we achieved a high diaphragm displacement. Additionally, Sateesh et al. (2018) simulated micro-pump was very small in size. It might be very difficult and costly to fabricate, because it requires higher spatial resolution fabrication techniques, while the two micro-pumps in this study were fabricated proportionally to the fabrication technology and commercially available materials. In the light of these findings, we may conclude that a BDM with two piezoelectric actuators might be a good candidate to be used in biomedical applications after further analyses and advanced fabrication technologies.

Table 4.1. Comparison with the state of the art

Ref.	Design Parameters	Figure	Explanation
[174]	Valveless, nine piezoelectric actuators, single chamber, silicone membrane.	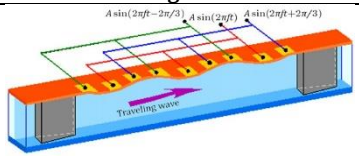	Upper diaphragm was unable to apply pressure to the fluid in the bottom of the chamber.
[175]	Valveless, three piezoelectric actuators, three chambers, silicone membrane.	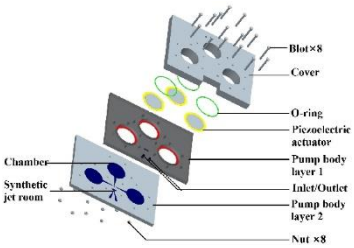	There was unwanted turbulence creating backpressure at output connection node.
[176]	Valveless, single piezoelectric actuator, single chamber, glass membrane.	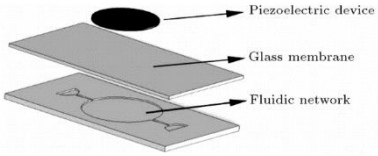	Low displacement values.
[177]	Valveless, single piezoelectric actuator, single chamber, PDMS membrane.	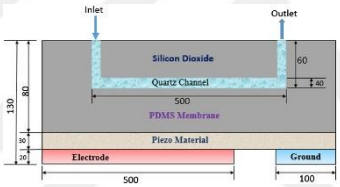	Very small channel size, very low flow rate.
Our work	Valveless, piezoelectric actuators, single chamber, silicone membrane.	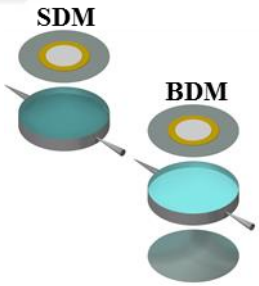	High flow rate at low voltage and frequency. BDM has improved flow rate by double diaphragm on a single chamber, easy to produce by rapid prototyping due to size.

The presented micro-pumps in this study were designed as potential candidate for biomedical applications which require relatively low level of driving voltages and frequencies. Insulin delivery or other fluidic drugs dispersion into the human body might be possible by these micro-pump designs. Table 4.2 shows the similar studies about the piezoelectric micro-pumps and their flow rates during the last 10 years. These studies include the micro-pumps with larger piezoelectric actuator and larger chambers. In addition, unlike our designs, they used higher voltages and frequencies. Thereby, some of the studies created higher flow rates.

Table 4.2. Summaries of experimental studies and findings in open literature

Ref.	Valves type	Piezoelectrics and size (mm)	Chambers and size (mm)	Diaphragm material	Voltage (V)	Freq. (Hz)	Q (ml/min)
[160]	Check-valve	1 Φ35 mm	1 n/r	n/r	150	30	26.55
[161]	Check-valve	2 Φ35 mm	1 n/r	Unused	200	15	45.98
[162]	Check-valve	1 30×15×0.4	1 Φ 10mm	Rubber	400	490	105
[163]	Check-valve	1 Φ35 mm	1 Φ34 mm	Unused	±70	25	196
[164]	Check-valve	1 22×40×0.7	1 Φ 10mm	Silicon	80	20	6.21
[165]	Check-valve	1 110×20×0.8	1 20×20×13.7	Silicon	400	445.5	163.7
[166]	Valveless	2 Φ 20mm	1 40×40×10	PT	±70	70	9.1
[167]	Check-valve	1 n/r	1 25×25×4.8	Resin	250	60	10
[168]	Check-valve	26 10×10×0.7	1 Φ 24mm	Kapton	400	750	187.2
SDM	Valveless	1 Φ 14mm	1 Φ 25mm	Silicon	45	20	32.85
BDM	Valveless	2 Φ 14mm	1 Φ 25mm	Silicon	45	20	35.4

When the studies in Table 4.2 were investigated, it was seen that Zhang et al. (2013a and 2013b) [160, 161], Pan et al. (2015) [165], Okura et al. (2017) [167] and Ye et al. (2018) [168] used very high AC voltages between 150 V and 400 V. These driving AC voltage levels can be considered very high and risky when the micro-pumps were considered to be used near the body surface for biomedical related applications. In addition, all the studies mentioned above used a check-valve in their designs. In the study by Ma et al. (2015a) [163], they used 70 V AC voltage at 25 Hz and they measured 196 ml/min net flow rate. In their study, the diameter of piezoelectric actuator was 2.5 time larger than we used in SDM and BDM micro-pump. Thereby, the maximum flow rate was almost 2.5 times higher according to our results. In fact, they did not show the calibration flow rate calculation and subtraction from the net flow rate values when the driving voltage was zero (at static condition). In addition, Ma et al. (2015b and 2016) [164, 166] used relatively low driving voltages (70-80 V) and frequency (20 Hz). But in these studies, they measured low net flow rates, i.e. 6.21 ml/min and 9.1 ml/min respectively. The most similar study to this presented study was done by Ma et. al (2016) [166] with a valveless geometry. Even though they used similar size piezoelectric actuator, their chamber height was 2.5 times bigger than our SDM and BDM micro-pump chambers. Thereby, they measured 2.5 times lower flow rates as compatible with the literature because of the chamber height effect [178, 179].

When these studies are considered in general, we see that we have obtained a high flow rate at lower voltage and frequency values by using an integrated reservoir with SDM and BDM designs.

4.5.2. Biomedical considerations of micro-pumps

Micro-pumps are one of the most important MEMS devices that can play an important role in drug delivering. The micro-pumps that are designed for the purpose of drug delivery should meet the requirements and basic terms, including drug biocompatibility, actuation safety, desired and controllable flow rate, small chip size and low power consumption. Biocompatibility is a very important key parameter that is necessarily considered for drug delivery micro-pumps [180, 181]. On the other hand, the micro-pumps used for the purpose of drug delivery in the human body should be selected so that they had biocompatibility and biostability [182]. Moreover, the implanted micro-pump based drug delivery system should have sufficient resistance to the physiological environment and the adverse impact of surrounding tissues [183].

Silicon is a good biocompatible material. It is one of the materials which has been much preferred in recent years' biomedical studies [184]. However, the process of using polymers in medical fields is widespread and suitable for human implantation. Additionally, polymer materials such as PMMA, PDMS, and SU-8 photo resist have better biocompatibility and are more preferred in micro-pump based drug delivery [185]. It might be concluded that micro-pump designs in this study were compatible with medical considerations.

CHAPTER 5. CONCLUSIONS AND FUTURE RESEARCH

The flow rate is limited in the single diaphragm micro-pumps. Thus, studies on multi-diaphragm micro-pumps are necessary. In multi-diaphragm micro-pumps, it is possible to achieve characteristics such as high flow rate, high pressure and good stability. The purpose of this study was to investigate the effect of electro-mechanical factors on flow rate. SDM and BDM were two novel designs that proposed in this study. The static displacements of multi-layer piezoelectric actuators of these micro-pumps were investigated. In addition, an analytical static displacement model of a multi-layer actuator with silicon layer at its bottom was developed. By using multi-layer laminated plate theory, fourth order partial differential equations derived from moment equilibrium equations were solved. Transverse and lateral displacements were obtained as a function of voltage and fluid pressure. Analytical displacement model was confirmed by experimental and finite element analyses. Analytical displacement model can be used for optimization and improvement of micro-pump performance and in designing diaphragm type in the multi-layer piezoelectric actuators of micro-pumps.

The effect of voltage and frequency was clearly shown on the flow rates. The embedded reservoir combined with the chambers were presented promising results. Materials were biocompatible which considered as a crucial factor for biomedical applications. The flow rates were comparable with the state-of-the-art literature. The SDM flow rate was increased by 37.73% at 10 Hz, 47% at 15 Hz and 52.06% at 20 Hz compared to 5 Hz reference excitation frequency. Moreover, as for BDM flow rates, the increment rates were 33.70%, 42.90% and 47.93% for the same frequencies. Both SDM and BDM flow rates were linearly increased as a function of voltages at all frequencies. Eventually, experimental results showed that novel BDM design will be a good candidate especially for biomedical applications, such as drug delivery, blood transport and body fluid vacuum after more investigations.

In this study, water was used as fluid. In fact, eye drops, drugs and blood have different components from water, which changes mechanical properties of the fluid. Even though there are many studies using water as fluid in the literature, the mechanical differences may significantly change the behaviour of the micro-pumps. This constitutes a limitation of our current study. After having the parameters about the eye drop, similar analyses will be applied in future studies. Throughout the study, effects of geometrical factors on flow rates were indicated. After miniaturizing, it will have significant contribution in clinical applications such as fluid transfer through a catheter, laparoscopic needles within the body.

REFERENCES

[1] Li, Y., Van Roy, W., Vereecken, P. M., Lagae, L., Effects of laminar flow within a versatile microfluidic chip for in-situ electrode characterization and fuel cells. Microelectron. Eng., 181, 47–54, 2017.

[2] Yang, R.-J., Liu, C.-C., Wang, Y.-N., Hou, H.-H., Fu, L.-M., A comprehensive review of micro-distillation methods. Chem. Eng. J., 313, 1509–1520, 2017.

[3] Mohith, S., Karanth, P. N., Kulkarni, S. M., Recent trends in mechanical micropumps and their applications: A review. Mechatronics, 60, 34–55, 2019.

[4] Kohl, M., Dittmann, D., Quandt, E., Winzek, B., Thin film shape memory microvalves with adjustable operation temperature. Sensors Actuators A Phys., 83(1–3), 214–219, 2000.

[5] Yang, Z., Matsumoto, S., Goto, H., Matsumoto, M., Maeda, R., Ultrasonic micromixer for microfluidic systems. Sensors Actuators A Phys., 93(3), 266–272, 2001.

[6] Baechi, D., Buser, R., Dual, J., A high density microchannel network with integrated valves and photodiodes. Sensors Actuators A Phys., 95(2–3), 77–83, 2002.

[7] Bedö, G., Fannasch, H., Müller, R., A silicon flow sensor for gases and liquids using AC measurements. Sensors Actuators A Phys., 85(1–3), 124–132, 2000.

[8] Brand, S., Microdosing systems: micropumps the beating heart of microfluidics. http://www.mstonline.de/news/events/micropumps, 2006.

[9] Pan, L., Deng, J., Yuan, D., Chen, D., Zhang, J., Numerical simulation of a thermal-bubble actuated diffuser-nozzle valveless pump. Sci. China Ser. E Technol. Sci., 52(10), 2967–2972, 2009.

[10] Munas, F. R., Amarasinghe, Y. W. R., Dao, D., Review on MEMS based micropumps for biomedical applications. Int. J. Innov. Res. Sci. Eng. Technol., 4, 5602-5615, 2015.

[11] Singhal, V., Garimella, S. V., Induction electrohydrodynamics micropump for high heat flux cooling. Sensors Actuators A Phys., 134(2), 650–659, 2007.

[12] Doll, A., Goldschmidtböing, F., Heinrichs, M., Woias, P., Schrag, H. J., Hopt, U. T., A piezoelectric bidirectional micropump for a medical application. In ASME 2004 International Mechanical Engineering Congress and Exposition, California, 151–159, 2004.

[13] Kim, J.-H., Kang, C. J., Kim, Y.-S., A disposable polydimethylsiloxane-based diffuser micropump actuated by piezoelectric-disc. Microelectron. Eng., 71(2), 119–124, 2004.

[14] Jang, J., Lee, S. S., Theoretical and experimental study of MHD (magnetohydrodynamic) micropump. Sensors Actuators A Phys., 80(1), 84–89, 2000.

[15] Zordan, E., Amirouche, F., Zhou, Y., Principle design and actuation of a dual chamber electromagnetic micropump with coaxial cantilever valves. Biomed. Microdevices, 12(1), 55–62, 2010.

[16] Wang, X., Cheng, C., Wang, S., Liu, S., Electroosmotic pumps and their applications in microfluidic systems. Microfluid. Nanofluidics, 6(2), 145–162, 2009.

[17] Smits, J.G., Vitafin, N.V., Piezo-electrical micropump. Eur. Pat. EP0134614, Netherlands, 1984.

[18] Yong-li, Z., Jian-kang, W., Numerical study of periodical flows of piezoelectric valveless micropump for biochips. Appl. Math. Mech., 26(8), 1026–1033, 2005.

[19] Abhari, F., Jaafar, H., Yunus, N.A.M., A comprehensive study of micropumps technologies. Int. J. Electrochem. Sci, 7(10), 9765–9780, 2012.

[20] Wang, Y.-N., Fu, L.-M., Micropumps and biomedical applications-A review. Microelectron. Eng., 195, 121-138, 2018.

[21] Yildirim, Y.A., Toprak, A., Tigli, O., Piezoelectric membrane actuators for micropump applications using PVDF-TrFE. J. Microelectromechanical Syst., 27(1), 86–94, 2018.

[22] Uhlig, S., Gaudet, M., Langa, S., Schimmanz, K., Conrad, H., Kaiser, B., Schenk, H., Electrostatically driven in-plane silicon micropump for modular configuration. Micromachines, 9(4), 1–15, 2018.

[23] Rusli, M.Q.A., Chee, P.S., Arsat, R., Lau, K.X., Leow, P.L., Electromagnetic actuation dual-chamber bidirectional flow micropump. Sensors Actuators A Phys., 282, 17–27, 2018.

[24] Cheong, H.R., Lai, K.C., Chee, P.S., A wireless powered electroactive polymer using magnetic resonant coupling. In IOP Conference Series: Materials Science and Engineering, 409(1), 1–6, 2018.

[25] Chee, P.S., Nafea, M., Leow, P.L., Ali, M.S.M., Thermal analysis of wirelessly powered thermo-pneumatic micropump based on planar LC circuit. J. Mech. Sci. Technol., 30(6), 2659–2665, 2016.

[26] Tripathi, D., Sharma, A., Bég, O.A., Electrothermal transport of nanofluids via peristaltic pumping in a finite micro-channel: Effects of Joule heating and Helmholtz-Smoluchowski velocity. Int. J. Heat Mass Transf., 111, 138–149, 2017.

[27] Guerine, A., Merzouki, T., El Hami, A., Ben Zineb, T., Uncertainty analysis of an actuator for a shape memory alloy micro-pump with uncertain parameters. Adv. Eng. Softw., 122, 22–30, 2018.

[28] Hasan, M.I., Ali, A.J.F., Tufah, R.S., Numerical study of the effect of channel geometry on the performance of Magnetohydrodynamic micro pump. Eng. Sci. Technol. an Int. J., 20(3), 982–989, 2017.

[29] Russel, M.K., Selvaganapathy, P.R., Ching, C.Y., Ion drag electrohydrodynamic (EHD) micro-pumps under a pulsed voltage. J. Electrostat., 82, 48–54, 2016.

[30] Li, L., Wang, X., Pu, Q., Liu, S., Advancement of electroosmotic pump in microflow analysis: A REVIEW. Anal. Chim. Acta, 1060, 1–16, 2019.

[31] Uvarov, I.V., Lemekhov, S.S., Melenev, A.E., Svetovoy, V.B., Exploding microbubbles driving a simple electrochemical micropump. J. Micromechanics Microengineering, 27(10), 1–7, 2017.

[32] Nie, C., Frijns, A.J.H., Mandamparambil, R., den Toonder, J.M.J., A microfluidic device based on an evaporation-driven micropump. Biomed. Microdevices, 17(2), 1–12, 2015.

[33] Yoon, E., Yun, K.-S., Micropump driven by movement of liquid drop induced by continuous electrowetting. U.S. Patent No. 6,629,826, Washington, DC: U.S. Patent and Trademark Office, 2003.

[34] Uvarov, I.V., Lemekhov, S.S., Melenev, A.E., Naumov, V.V., Koroleva, O.M., Izyumov, M.O., Svetovoy, V.B., A simple electrochemical micropump: design and fabrication. In Journal of Physics: Conference Series, 741(1), 1–6, 2016.

[35] Wenzel, S.W., Costello, B.J., Micropump. U.S. Patent No. 6,720,710, Washington, DC: U.S. Patent and Trademark Office, 2004.

[36] Nguyen, N.-T., Huang, X., Chuan, T.K., MEMS-micropumps: a review. J. Fluids Eng., 124(2), 384–392, 2002.

[37] Kim, H., Astle, A.A., Najafi, K., Bernal, L.P., Washabaugh, P.D., An integrated electrostatic peristaltic 18-stage gas micropump with active microvalves. J. Microelectromechanical Syst., 24(1), 192–206, 2015.

[38] Ghazali, F.A.M., Mah, C.K., AbuZaiter, A., Chee, P.S., Ali, M.S.M., Soft dielectric elastomer actuator micropump. Sensors Actuators A Phys., 263, 276–284, 2017.

[39] Bar-Cohen, Y., Zhang, Q., Electroactive polymer actuators and sensors. MRS Bull., 33(3), 173–181, 2008.

[40] Nam, D.N.C., Ahn, K.K., Design of an IPMC diaphragm for micropump application. Sensors Actuators A Phys., 187, 174–182, 2012.

[41] Khawwaf, J., Zheng, J., Lu, R., Al-Ghanimi, A., Kazem, B.I., Man, Z., Robust tracking control of an IPMC actuator using nonsingular terminal sliding mode. Smart Mater. Struct., 26(9), 1–10, 2017.

[42] Mohd Said, M., Yunas, J., Bais, B., Hamzah, A., Yeop Majlis, B., The Design, Fabrication, and Testing of an Electromagnetic Micropump with a Matrix-Patterned Magnetic Polymer Composite Actuator Membrane. Micromachines, 9(1), 1–10, 2017.

[43] Sima, A.H., Salari, A., Shafii, M.B., Low-cost reciprocating electromagnetic-based micropump for high-flow rate applications. J. Micro/Nanolithography, MEMS, MOEMS, 14(3), 035003, 2015.

[44] Chee, P.S., Minjal, M.N., Leow, P.L., Ali, M.S.M., Wireless powered thermo-pneumatic micropump using frequency-controlled heater. Sensors Actuators A Phys., 233, 1–8, 2015.

[45] Benard, W.L., Kahn, H., Heuer, A.H., Huff, M.A., Thin-film shape-memory alloy actuated micropumps. J. Microelectromechanical Syst., 7(2), 245–251, 1998.

[46] Bonk, S., Stubbe, M., Buehler, S., Tautorat, C., Baumann, W., Klinkenberg, E.D., Gimsa, J., Design and characterization of a sensorized microfluidic cell-culture system with electro-thermal micro-pumps and sensors for cell adhesion, oxygen, and pH on a glass chip. Biosensors, 5(3), 513–536, 2015.

[47] van den Berg, A., Lammerink, T.S.J., Micro total analysis systems: microfluidic aspects, integration concept and applications. In Microsystem technology in chemistry and life science. Springer, Berlin, Heidelberg, 21–49, 1998.

[48] Fong, J., Xiao, Z., Takahata, K., Wireless implantable chip with integrated nitinol-based pump for radio-controlled local drug delivery. Lab Chip, 15(4), 1050–1058, 2015.

[49] Ali, M.S.M., Takahata, K., Wireless microfluidic control with integrated shape-memory-alloy actuators operated by field frequency modulation. J. Micromechanics Microengineering, 21(7), 1–10, 2011.

[50] Spieth, S., Schumacher, A., Kallenbach, C., Messner, S., Zengerle, R., The NeuroMedicator—a micropump integrated with silicon microprobes for drug delivery in neural research. J. Micromechanics Microengineering, 22(6), 1–11, 2012.

[51] Spieth, S., Schumacher, A., Holtzman, T., Rich, P.D., Theobald, D.E., Dalley, J.W., Nouna, R., Messner, S., Zengerle, R, An intra-cerebral drug delivery system for freely moving animals. Biomed. Microdevices, 14(5), 799–809, 2012.

[52] Duwairi, H., Abdullah, M., Thermal and flow analysis of a magneto-hydrodynamic micropump. Microsyst. Technol., 13(1), 33–39, 2007.

[53] Sato, T., Yamanishi, Y., Cacucciolo, V., Kuwajima, Y., Shigemune, H., Cianchetti, M., Laschi, C., Maeda, S., Electrohydrodynamic conduction pump with asymmetrical electrode structures in the microchannels. Chem. Lett., 46(7), 950–952, 2017.

[54] Russel, M.K., Hasnain, S.M., Selvaganapathy, P.R., Ching, C.Y., Effect of doping ferrocene in the working fluid of electrohydrodynamic (EHD) micropumps. Microfluid. Nanofluidics, 20(8), 1–9, 2016.

[55] Chen, C.-H., Santiago, J.G., A planar electroosmotic micropump. J. Microelectromechanical Syst., 11(6), 672–683, 2002.

[56] Lin, S.-C., Lu, J.-C., Sung, Y.-L., Lin, C.-T., Tung, Y.-C., A low sample volume particle separation device with electrokinetic pumping based on circular travelling-wave electroosmosis. Lab Chip, 13(15), 3082–3089, 2013.

[57] Liu, B., Sun, J., Li, D., Zhe, J., Oh, K. W., A high flow rate thermal bubble-driven micropump with induction heating. Microfluid. Nanofluidics, 20(11), 1–9, 2016.

[58] Zhang, H., Xin, F.U., Zhen-Jun, Z.H.U., A microfluidic microbeads array chip integrated with micro-fluid driven micro-pump for discrimination of gene mutation. Chinese J. Anal. Chem., 41(4), 473–480, 2013.

[59] Kim, H., Kim, K., Lee, S.J., Compact and thermosensitive nature-inspired micropump. Sci. Rep., 6, 1–10, 2016.

[60] Javadi, A., Habibi, M., Taheri, F.S., Moulinet, S., Bonn, D., Effect of wetting on capillary pumping in microchannels. Sci. Rep., 3, 1–6, 2013.

[61] Kjeang, E., Djilali, N., Sinton, D., Microfluidic fuel cells: A review. J. Power Sources, 186(2), 353–369, 2009.

[62] Meng, A.H., Nguyen, N.-T., White, R.M., Focused flow micropump using ultrasonic flexural plate waves. Biomed. Microdevices, 2(3), 169–174, 2000.

[63] Dereshgi, H.A., Yildiz, M.Z., A novel micropump design: Investigation of the voltage effect on the net flow rate. Sakarya University Journal of Science, 22(4), 1152–1156, 2018.

[64] Dereshgi, H.A., Yildiz, M.Z., Investigation of electro-mechanical factors effecting piezoelectric actuator for valveless micropump characteristics. J. Eng. Sci. Technol., 13(9), 2843–2856, 2018.

[65] Farshchi Yazdi, S.A.F., Corigliano, A., Ardito, R., 3-D Design and Simulation of a Piezoelectric Micropump. Micromachines, 10(4), 1–17, 2019.

[66] Wang, J., Liu, Y., Shen, Y., Chen, S., Yang, Z., A Resonant Piezoelectric Diaphragm Pump Transferring Gas with Compact Structure. Micromachines, 7(12), 1–9, 2016.

[67] Pabst, O., Perelaer, J., Beckert, E., Schubert, U.S., Eberhardt, R., Tünnermann, A., All inkjet-printed piezoelectric polymer actuators: Characterization and applications for micropumps in lab-on-a-chip systems. Org. Electron., 14(12), 3423–3429, 2013.

[68] Pabst, O., Hölzer, S., Beckert, E., Perelaer, J., Schubert, U.S., Eberhardt, R., Tünnermann, A., Inkjet printed micropump actuator based on piezoelectric polymers: Device performance and morphology studies. Org. Electron., 15(11), 3306–3315, 2014.

[69] Le, S., Hegab, H., Investigation of a multistage micro gas compressor cascaded in series for increase pressure rise. Sensors Actuators A Phys., 256, 66–76, 2017.

[70] Dong, J.S., Liu, R.G., Liu, W.S., Chen, Q.Q., Yang, Y., Wu, Y., Yang, Z.G., Lin, B.S., Design of a piezoelectric pump with dual vibrators. Sensors Actuators A Phys., 257, 165–172, 2017.

[71] Johnson, D., Borkholder, D., Towards an implantable, low flow micropump that uses no power in the blocked-flow state. Micromachines, 7(6), 1–16, 2016.

[72] Shoji, E., Fabrication of a diaphragm micropump system utilizing the ionomer-based polymer actuator. Sensors Actuators B Chem., 237, 660–665, 2016.

[73] Tanaka, Y., Noguchi, Y., Yalikun, Y., Kamamichi, N., Earthworm muscle driven bio-micropump. Sensors Actuators B Chem., 242, 1186–1192, 2017.

[74] Hamid, N.A., Majlis, B.Y., Yunas, J., Syafeeza, A.R., Wong, Y.C., Ibrahim, M., A stack bonded thermo-pneumatic micro-pump utilizing polyimide based actuator membrane for biomedical applications. Microsyst. Technol., 23(9), 4037–4043, 2017.

[75] Robertson, J.M., Rodriguez, R.X., Holmes Jr, L.R., Mather, P.T., Wetzel, E.D., Thermally driven microfluidic pumping via reversible shape memory polymers. Smart Mater. Struct., 25(8), 1–13, 2016.

[76] Shaegh, S.A.M., Wang, Z., Ng, S.H., Wu, R., Nguyen, H.T., Chan, L.C.Z., Toh, A.G.G., Wang, Z., Plug-and-play microvalve and micropump for rapid integration with microfluidic chips. Microfluid. Nanofluidics, 19(3), 557–564, 2015.

[77] Kawun, P., Leahy, S., Lai, Y., A thin PDMS nozzle/diffuser micropump for biomedical applications. Sensors Actuators A Phys., 249, 149–154, 2016.

[78] Zhou, Y., Amirouche, F., An electromagnetically-actuated all-PDMS valveless micropump for drug delivery. Micromachines, 2(3), 345–355, 2011.

[79] Ehsani, A., Nejat, A., Conceptual design and performance analysis of a novel flexible-valve micropump using magneto-fluid--solid interaction. Smart Mater. Struct., 26(5), 1–12, 2017.

[80] Fadl, A., Zhang, Z., Geller, S., Tölke, J., Krafczyk, M., Meyer, D., The effect of the microfluidic diodicity on the efficiency of valve-less rectification micropumps using Lattice Boltzmann Method. Microsyst. Technol., 15(9), 1379–1387, 2009.

[81] Zhang, R., You, F., Lv, Z., He, Z., Wang, H., Huang, L., Development and characterization a single-active-chamber piezoelectric membrane pump with multiple passive check valves. Sensors, 16(12), 1–12, 2016.

[82] Revathi, S., Padmapriya, N., Padmanabhan, R., A design analysis of piezoelectric-polymer composite-based valveless micropump. Int. J. Model. Simul., 39(2), 110–124, 2018.

[83] Chen, S., Liu, Y., Shen, Y., Wang, J., Yang, Z., The structure of wheel check valve influence on air block phenomenon of piezoelectric micro-pump. Micromachines, 6(11), 1745–1754, 2015.

[84] Sim, W.Y., Yoon, H.J., Jeong, O.C., Yang, S.S., A phase-change type micropump with aluminum flap valves. J. Micromechanics Microengineering, 13(2), 286–294, 2003.

[85] Pan, T., McDonald, S.J., Kai, E.M., Ziaie, B., A magnetically driven PDMS micropump with ball check-valves. J. Micromechanics Microengineering, 15(5), 1021–1026, 2005.

[86] Dau, V.T., Dinh, T.X., Katsuhiko, T., Susumu, S., A cross-junction channel valveless-micropump with PZT actuation. Microsyst. Technol., 15(7), 1039–1044, 2009.

[87] Olsson, A., Stemme, G., Stemme, E., A valve-less planar fluid pump with two pump chambers. Sensors Actuators A Phys., 47(1–3), 549–556, 1995.

[88] Wang, T., He, J., An, C., Wang, J., Lv, L., Luo, W., Wu, C., Shuai, Y., Zhang, W., Lee, C., Study of the vortex based virtual valve micropump. J. Micromechanics Microengineering, 28(12), 1–8, 2018.

[89] Izzo, I., Accoto, D., Menciassi, A., Schmitt, L., Dario, P., Modeling and experimental validation of a piezoelectric micropump with novel no-moving-part valves. Sensors Actuators A Phys., 133(1), 128–140, 2007.

[90] Dau, V.T., Dinh, T.X., Sugiyama, S., A MEMS-based silicon micropump with intersecting channels and integrated hotwires. J. Micromechanics Microengineering, 19(12), 1–7, 2009.

[91] Stemme, E., Stemme, G., A valveless diffuser/nozzle-based fluid pump. Sensors Actuators A Phys., 39(2), 159–167, 1993.

[92] Derakhshan, S., Beigzadeh, B., Rashidi, M., Pourrahmani, H., Performance Improvement and Two-Phase Flow Study of a Piezoelectric Micropump with Tesla Nozzle-Diffuser Microvalves. J. Appl. Fluid Mech., 12(2), 341-350, 2019.

[93] Gidde, R.R., Pawar, P.M., Ronge, B.P., Dhamgaye, V.P., Design optimization of an electromagnetic actuation based valveless micropump for drug delivery application. Microsyst. Technol., 25(2), 509–519, 2019.

[94] Qian, J., Chen, M., Liu, X., Jin, Z., A numerical investigation of the flow of nanofluids through a micro Tesla valve. J. Zhejiang Univ. A, 20(1), 50–60, 2019.

[95] Nobakht, A.Y., Shahsavan, M., Paykani, A., Numerical study of diodicity mechanism in different Tesla-type microvalves. J. Appl. Res. Technol., 11(6), 876–885, 2013.

[96] de Vries, S.F., Florea, D., Homburg, F.G.A., Frijns, A.J.H., Design and operation of a Tesla-type valve for pulsating heat pipes. Int. J. Heat Mass Transf., 105, 1–11, 2017.

[97] Mohammadzadeh, K., Kolahdouz, E.M., Shirani, E., Shafii, M.B., Numerical study on the performance of Tesla type microvalve in a valveless micropump in the range of low frequencies. J. Micro-Bio Robot., 8(3–4), 145–159, 2013.

[98] Bardell, R.L., The diodicity mechanism of Tesla-type no-moving-parts valves. University of Washington, Graduate School, Department of Mechanical Engineering, Ph.D. Thesis, 2000.

[99] Olsson, A., Stemme, G., Stemme, E., Simulation studies of diffuser and nozzle elements for valve-less micropumps. In Proceedings of International Solid State Sensors and Actuators Conference (Transducers' 97), Chicago, 1039–1042, 1997.

[100] Mohammadzadeh, K., Kolahdouz, E.M., Shirani, E., Numerical study on the effect of the number of stages on the performance of Tesla microvalve and comparison with nozzle/diffuser microvalve. Modares Mech. Eng., 12(6), 124–135, 2013.

[101] Yamahata, C., Lotto, C., Al-Assaf, E., Gijs, M.A.M., A PMMA valveless micropump using electromagnetic actuation. Microfluid. Nanofluidics, 1(3), 197–207, 2005.

[102] Jeong, O.C., Park, S.W., Yang, S.S., Pak, J.J., Fabrication of a peristaltic PDMS micropump. Sensors Actuators A Phys., 123, 453–458, 2005.

[103] Ahn, C.H., Allen, M.G., Fluid micropumps based on rotary magnetic actuators. In Proceedings IEEE Micro Electro Mechanical Systems, 408–412, 1995.

[104] Hsu, Y.-C., Lin, S.-J., Hou, C.-C., Development of peristaltic antithrombogenic micropumps for in vitro and ex vivo blood transportation tests. Microsyst. Technol., 14(1), 31–41, 2008.

[105] Amirouche, F., Zhou, Y., Johnson, T., Current micropump technologies and their biomedical applications. Microsyst. Technol., 15(5), 647–666, 2009.

[106] Cui, Q., Liu, C., Zha, X.F.W., Design and Simulation of a Piezoelectrically Actuated Micropump for the Drug Delivery System. In 2006 IEEE International Conference on Automation Science and Engineering, Shanghai, 45–50, 2006.

[107] Azarbadegan, A., Moeendarbary, E., Cortes-Quiroz, C.A., Eames, I., Investigation of double-chamber series valveless micropump: An analytical approach. In 2010 Fourth International Conference on Quantum, Nano and Micro Technologies, St. Maarten, 107–112, 2010.

[108] Huang, C.-W., Huang, S.-B., Lee, G.-B., Pneumatic micropumps with serially connected actuation chambers. J. micromechanics microengineering, 16(11), 2265–2272, 2006.

[109] Jang, L.-S., Kan, W.-H., Peristaltic piezoelectric micropump system for biomedical applications. Biomed. Microdevices, 9(4), 619–626, 2007.

[110] Shoji, S., Nakagawa, S., Esashi, M., Micropump and sample-injector for integrated chemical analyzing systems. Sensors Actuators A Phys., 21(1–3), 189–192, 1990.

[111] Shoji, S., Esashi, M., Matsuo, T., Prototype miniature blood gas analyser fabricated on a silicon wafer. Sensors and Actuators, 14(2), 101–107, 1988.

[112] Zdeblick, M.J., Angell, J.B., A microminiature electric-to-fluidic valve. The 4th International Conference Solid State Sensors and Actuators (Transducer ’87), Tokyo, 827–829, 1987.

[113] Dereshgi, H.A., Design of novel micro-pumps for mechatronic applications. In 4th Int. Symposium on Innovative Technologies in Engineering and Science (ISITES), Antalya, 1435–1447, 2016.

[114] Smits, J.G., Piezoelectric micropump with three valves working peristaltically. Sensors Actuators A Phys., 21(1–3), 203–206, 1990.

[115] Fournier, S., Chappel, E., Modeling of a piezoelectric MEMS micropump dedicated to insulin delivery and experimental validation using integrated pressure sensors: Application to partial occlusion management. J. Sensors, 2017, 1–7, 2017.

[116] Haldkar, R.K., Gupta, V.K., Sheorey, T., Modeling and flow analysis of piezoelectric based micropump with various shapes of microneedle. J. Mech. Sci. Technol., 31(6), 2933–2941, 2017.

[117] Wang, B., Chu, X., Li, E., Li, L., Simulations and analysis of a piezoelectric micropump. Ultrasonics, 44, e643--e646, 2006.

[118] Cui, Q., Liu, C., Zha, X.F., Study on a piezoelectric micropump for the controlled drug delivery system. Microfluid. Nanofluidics, 3(4), 377–390, 2007.

[119] Wang, X.Y., Ma, Y.T., Yan, G.Y., Feng, Z.H., A compact and high flow-rate piezoelectric micropump with a folded vibrator. Smart Mater. Struct., 23(11), 1–11, 2014.

[120] Singh, S., Kumar, N., George, D., Sen, A.K., Analytical modeling, simulations and experimental studies of a PZT actuated planar valveless PDMS micropump. Sensors Actuators A Phys., 225, 81–94, 2015.

[121] Fan, B., Song, G., Hussain, F., Simulation of a piezoelectrically actuated valveless micropump. Smart Mater. Struct., 14(2), 400–405, 2005.

[122] Wu, C.-L., Yang, J.-C., Chen, Y.-C., Low power consumption PZT actuated micro-pump. In 2006 International Microsystems, Package, Assembly Conference Taiwan, Taiwan, 1–4, 2006.

[123] Eladi, P.B., Chatterjee, D., DasGupta, A., Design and development of a piezoelectrically actuated micropump for drug delivery application. In Micro and Smart Devices and Systems, Springer, New Delhi, 127–141, 2014.

[124] Cazorla, P.H., Fuchs, O., Cochet, M., Maubert, S., Le Rhun, G., Fouillet, Y., Defay, E., A low voltage silicon micro-pump based on piezoelectric thin films. Sensors Actuators A Phys., 250, 35–39, 2016.

[125] Revathi, S., Padmanabhan, R., Design and Development of Piezoelectric Composite-Based Micropump. J. Microelectromechanical Syst., 27(6), 1105–1113, 2018.

[126] Li, S., Chen, S., Analytical analysis of a circular PZT actuator for valveless micropumps. Sensors Actuators A Phys., 104(2), 151–161, 2003.

[127] Mo, C., Wright, R., Slaughter, W.S., Clark, W.W., Behaviour of a unimorph circular piezoelectric actuator. Smart Mater. Struct., 15(4), 1094–1102, 2006.

[128] Dong, S., Uchino, K., Li, L., Viehland, D., Analytical solutions for the transverse deflection of a piezoelectric circular axisymmetric unimorph actuator. IEEE Trans. Ultrason. Ferroelectr. Freq. Control, 54(6), 1240–1249, 2007.

[129] Deshpande, M., Saggere, L., An analytical model and working equations for static deflections of a circular multi-layered diaphragm-type piezoelectric actuator. Sensors Actuators A Phys., 136(2), 673–689, 2007.

[130] Wang, D.H., Huo, J., Modeling and testing of the static deflections of circular piezoelectric unimorph actuators. J. Intell. Mater. Syst. Struct., 21(16), 1603–1616, 2010.

[131] Mohammadi, S., Abdalbeigi, M., Analytical optimization of piezoelectric circular diaphragm generator. Adv. Mater. Sci. Eng., 2013, 1–10, 2013.

[132] Oniszczuk, Z., Transverse vibrations of the elastically connected rectangular double-membrane compound system. J. Sound Vib., 221(2), 235–250, 1999.

[133] Pan, L.S., Ng, T.Y., Liu, G.R., Lam, K.Y., Jiang, T.Y., Analytical solutions for the dynamic analysis of a valveless micropump—a fluid--membrane coupling study. Sensors Actuators A Phys., 93(2), 173–181, 2001.

[134] Cho, J., Anderson, M., Richards, R., Bahr, D., Richards, C., Optimization of electromechanical coupling for a thin-film PZT membrane: II. Experiment. J. micromechanics microengineering, 15(10), 1804–1809, 2005.

[135] Yu, M., Balachandran, B., Sensor diaphragm under initial tension: linear analysis. Exp. Mech., 45(2), 123–129, 2005.

[136] Olfatnia, M., Singh, V.R., Xu, T., Miao, J.M., Ong, L.S., Analysis of the vibration modes of piezoelectric circular microdiaphragms. J. micromechanics microengineering, 20(8), 1–8, 2010.

[137] Kaviani, S., Bahrami, M., Esfahani, A.M., Parsi, B., A modeling and vibration analysis of a piezoelectric micro-pump diaphragm. Comptes Rendus Mécanique, 342(12), 692–699, 2014.

[138] Esfahani, A.M., Bahrami, M., Vibration analysis of a circular thin polymeric piezoelectric diaphragm with fluid interaction. Int. J. Mech. Mater. Des., 12(3), 401–411, 2016.

[139] Monemian Esfahani, A., Bahrami, M., Ghaffarian Anbarani, S.R., Forced transverse vibration analysis of a circular viscoelastic polymeric piezoelectric microplate with fluid interaction. Aust. J. Mech. Eng., 16(1), 31–42, 2018.

[140] He, X., Xu, W., Lin, N., Uzoejinwa, B.B., Deng, Z., Dynamics modeling and vibration analysis of a piezoelectric diaphragm applied in valveless micropump. J. Sound Vib., 405, 133–143, 2017.

[141] Hu, Y., Liang, X., Wang, W., A theoretical solution of resonant circular diaphragm-type piezoactuators with added mass loads. Sensors Actuators A Phys., 258, 74–87, 2017.

[142] Nguyen, T.T., Pham, M., Goo, N.S., Development of a peristaltic micropump for bio-medical applications based on mini LIPCA. J. Bionic Eng., 5(2), 135–141, 2008.

[143] Jang, L.-S., Yu, Y.-C., Peristaltic micropump system with piezoelectric actuators. Microsyst. Technol., 14(2), 241–248, 2008.

[144] Chao, C.-S., Huang, P.-C., Chen, M.-K., Jang, L.-S., Design and analysis of charge-recovery driving circuits for portable peristaltic micropumps with piezoelectric actuators. Sensors Actuators A Phys., 168(2), 313–319, 2011.

[145] Ma, T., Sun, S., Li, B., Chu, J., Piezoelectric peristaltic micropump integrated on a microfluidic chip. Sensors Actuators A Phys., 292, 90–96, 2019.

[146] Junwu, K., Zhigang, Y., Taijiang, P., Guangming, C., Boda, W., Design and test of a high-performance piezoelectric micropump for drug delivery. Sensors Actuators A Phys., 121(1), 156–161, 2005.

[147] Ma, H.-K., Hou, B.-R., Wu, H.Y., Lin, C.-Y., Gao, J.-J., Kou, M.-C., Development and application of a diaphragm micro-pump with piezoelectric device. Microsyst. Technol., 14(7), 1001–1007, 2008.

[148] Cheng, C.-H., Tseng, Y.-P., Characteristic studies of the piezoelectrically actuated micropump with check valve. Microsyst. Technol., 19(11), 1707–1715, 2013.

[149] Ren, Y.J., Ma, Y.T., Huang, D., Chen, J., Feng, Z.H., Elastic string check valves can efficiently heighten the piezoelectric pump's working frequency. Sensors Actuators A Phys., 244, 126–132, 2016.

[150] Forster, F.K., Bardell, R.L., Afromowitz, M.A., Sharma, N.R., Blanchard, A., Design, fabrication and testing of fixed-valve micro-pumps. ASME-PUBLICATIONS-FED, 234, 39–44, 1995.

[151] Forster, F.K., Williams, B.E., Parametric Design of Fixed-Geometry Microvalves: The Tesser Valve. In ASME 2002 International Mechanical Engineering Congress and Exposition, New Orleans, 431–437, 2002.

[152] Cui, Q., Liu, C., Zha, X.F., Simulation and optimization of a piezoelectric micropump for medical applications. Int. J. Adv. Manuf. Technol., 36(5–6), 516–524, 2008.

[153] Guan, Y., Ren, J., Zhang, G., Cheng, Z., Fabrication and experiment studies of the piezoelectric micropump with saw-tooth microchannel. In 2009 IEEE International Conference on Intelligent Computing and Intelligent Systems, Shanghai, 733–737, 2009.

[154] Ji, J., Chen, S., Xie, X., Wang, X., Kan, J., Zhang, Z., Li, J., Design and Experimental Verification on Characteristics of Valve-Less Piezoelectric Pump Effected by Valve Hole Spacing. IEEE Access, 7, 36259–36265, 2019.

[155] Van Lintel, H.T.G., de Pol, F.C.M., Bouwstra, S., A piezoelectric micropump based on micromachining of silicon. Sensors and actuators, 15(2), 153–167, 1988.

[156] Cao, L., Mantell, S., Polla, D., Design and simulation of an implantable medical drug delivery system using microelectromechanical systems technology. Sensors Actuators A Phys., 94(1–2), 117–125, 2001.

[157] Kan, J., Tang, K., Liu, G., Zhu, G., Shao, C., Development of serial-connection piezoelectric pumps. Sensors Actuators A Phys., 144(2), 321–327, 2008.

[158] Ma, H.K., Su, H.C., Wu, J.Y., Study of an innovative one-sided actuating piezoelectric valveless micropump with a secondary chamber. Sensors Actuators A Phys., 171(2), 297–305, 2011.

[159] Jang, L.S., Li, Y.J., Lin, S.J., Hsu, Y.C., Yao, W.S., Tsai, M.C., Hou, C.C., A stand-alone peristaltic micropump based on piezoelectric actuation. Biomed. Microdevices, 9(2), 185–194, 2007.

[160] Zhang, Z., Kan, J., Cheng, G., Wang, H., Jiang, Y., A piezoelectric micropump with an integrated sensor based on space-division multiplexing. Sensors Actuators A Phys., 203, 29–36, 2013.

[161] Zhang, Z., Kan, J., Wang, S., Wang, H., Wen, J., Ma, Z., Flow rate self-sensing of a pump with double piezoelectric actuators. Mech. Syst. Signal Process., 41(1–2), 639–648, 2013.

[162] Wang, X.Y., Ma, Y.T., Yan, G.Y., Huang, D., Feng, Z.H., High flow-rate piezoelectric micropump with two fixed ends polydimethylsiloxane valves and compressible spaces. Sensors Actuators A Phys., 218, 94–104, 2014.

[163] Ma, H.K., Chen, R.H., Hsu, Y.H., Development of a piezoelectric-driven miniature pump for biomedical applications. Sensors Actuators A Phys., 234, 23–33, 2015.

[164] Ma, H.-K., Luo, W.-F., Lin, J.-Y., Development of a piezoelectric micropump with novel separable design for medical applications. Sensors Actuators A Phys., 236, 57–66, 2015.

[165] Pan, Q.S., He, L.G., Huang, F.S., Wang, X.Y., Feng, Z.H., Piezoelectric micropump using dual-frequency drive. Sensors Actuators A Phys., 229, 86–93, 2015.

[166] Ma, H.K., Chen, R.H., Yu, N.S., Hsu, Y.H., A miniature circular pump with a piezoelectric bimorph and a disposable chamber for biomedical applications. Sensors Actuators A Phys., 251, 108–118, 2016.

[167] Okura, N., Nakashoji, Y., Koshirogane, T., Kondo, M., Tanaka, Y., Inoue, K., Hashimoto, M., A compact and facile microfluidic droplet creation device using a piezoelectric diaphragm micropump for droplet digital PCR platforms. Electrophoresis, 38(20), 2666–2672, 2017.

[168] Ye, Y., Chen, J., Ren, Y.J., Feng, Z.H., Valve improvement for high flow rate piezoelectric pump with PDMS film valves. Sensors Actuators A Phys., 283, 245–253, 2018.

[169] Yildiz, M.Z., Dereshgi, H.A., Design and analysis of PZT micropumps for biomedical applications: Glaucoma treatment. Journal of Engg. Research, 7(2), 202–217, 2019.

[170] Dereshgi, H.A., Yildiz, M.Z., Numerical Study of Novel MEMS-Based Valveless Piezoelectric Micropumps in the Range of Low Voltages and Frequencies. In 2019 Scientific Meeting on Electrical-Electronics & Biomedical Engineering and Computer Science (EBBT), Istanbul, 1–4, 2019.

[171] Singhal, V., Garimella, S.V., Murthy, J.Y., Low Reynolds number flow through nozzle-diffuser elements in valveless micropumps. Sensors Actuators A Phys., 113(2), 226–235, 2004.

[172] Olsson, A., Stemme, G., Stemme, E., Numerical and experimental studies of flat-walled diffuser elements for valve-less micropumps. Sensors Actuators A Phys., 84(1–2), 165–175, 2000.

[173] Holman, J.P., Experimental Methods for Engineers. Sixth ed., McGraw Hill, New York, 1994.

[174] Afrasiab, H., Movahhedy, M.R., Assempour, A., Proposal of a new design for valveless micropumps. Sci. Iran., 18(6), 1261–1266, 2011.

[175] He, X., Xu, L., Zhang, X., Yang, S., A bidirectional valveless piezoelectric micropump with three chambers applying synthetic jet. J. Mech. Sci. Technol., 30(9), 4015–4022, 2016.

[176] Kolahdouz, E.M., Mohammadzadeh, K., Shirani, E., Ziaei-Rad, S., Performance of piezoelectrically actuated micropump with different driving voltage shapes and frequencies. Sci. Iran. Trans. B, Mech. Eng., 21(5), 1635–1642, 2014.

[177] Sateesh, J., Sravani, K.G., Kumar, R.A., Guha, K., Rao, K.S., Design and flow analysis of MEMS based piezo-electric micro pump. Microsyst. Technol., 24(3), 1609–1614, 2018.

[178] Ni, J., Huang, F., Wang, B., Li, B., Lin, Q., A planar PDMS micropump using in-contact minimized-leakage check valves. J. micromechanics microengineering, 20(9), 1–7, 2010.

[179] Lin, Q., Yang, B., Xie, J., Tai, Y.-C., Dynamic simulation of a peristaltic micropump considering coupled fluid flow and structural motion. J. Micromechanics Microengineering, 17(2), 220–228, 2006.

[180] Lins, G., Skogberg, L., An investigation of insulin pump therapy and evaluation of using a micropump in a future insulin pump. KTH, M.S. thesis, 2001.

[181] Grayson, A.C.R., Shawgo, R.S., Johnson, A.M., Flynn, N.T., Li, Y., Cima, M.J., Langer, R., A BioMEMS review: MEMS technology for physiologically integrated devices. Proc. IEEE, 92(1), 6–21, 2004.

[182] Anderson, J.M., Langone, J.J., Issues and perspectives on the biocompatibility and immunotoxicity evaluation of implanted controlled release systems. J. Control. release, 57(2), 107–113, 1999.

[183] Anderson, J.M., Inflammation, Wound Healing and the Foreign Body Response Biomaterials Science: An Introduction to Materials in Medicine. Academic Press Inc., San Diego, CA, 1996.

[184] Dereshgi, H.A., Yildiz, M.Z., Parlak, N., Performance Comparison of Novel Single and Bi-Diaphragm PZT Based Valveless Micropumps. J. Appl. Fluid Mech., 13(2), 401-412, 2020.

[185] Nisar, A., Afzulpurkar, N., Mahaisavariya, B., Tuantranont, A., MEMS-based micropumps in drug delivery and biomedical applications. Sensors Actuators B Chem., 130(2), 917–942, 2008.

RESUME

Hamid ASADI DERESHGI received the MSc degree in Mechatronics Engineering from Islamic Azad University, Kashan, Iran, in 2013. He is currently a Ph.D. candidate in Mechatronics Engineering at Sakarya University, Turkey. He is also a member of the Biomedical Research Laboratory at Sakarya Applied Sciences University. His research interests are finite element modelling of materials, micro/nano electromechancial systems, microfluidics, biomedical instrumentation.